

## Original Article

**Cite this article:** Landing E, Schmitz MD, Geyer G, Traylor RB, and Bowring SA (2021) Precise early Cambrian U–Pb zircon dates bracket the oldest trilobites and archaeocyaths in Moroccan West Gondwana. *Geological Magazine* **158**: 219–238. <https://doi.org/10.1017/S0016756820000369>

Received: 14 November 2019

Revised: 9 March 2020

Accepted: 6 April 2020

First published online: 15 June 2020

**Keywords:**


Lower Cambrian; U–Pb dates; Morocco; oldest trilobites; palaeogeography

**Author for correspondence:**

Ed Landing, Email: [ed.landing@nyused.gov](mailto:ed.landing@nyused.gov)

<sup>†</sup>Deceased

# Precise early Cambrian U–Pb zircon dates bracket the oldest trilobites and archaeocyaths in Moroccan West Gondwana

Ed Landing<sup>1</sup> , Mark D. Schmitz<sup>2</sup>, Gerd Geyer<sup>3</sup> , Robin B. Traylor<sup>2,4</sup> and Samuel A. Bowring<sup>5,†</sup>

<sup>1</sup>New York State Museum, 222 Madison Avenue, Albany, NY 12230, USA; <sup>2</sup>Department of Geosciences, Boise State University, 1910 University Drive, Boise, Idaho 83725, USA; <sup>3</sup>Lehrstuhl für Geodynamik und Geomaterialforschung, Institut für Geographie und Geologie, Bayerische Julius-Maximilians-Universität Würzburg, Am Hubland, 97074 Würzburg, Germany; <sup>4</sup>Present address: Department of Life and Environmental Sciences, University of California–Merced, Merced, CA 95343, USA and <sup>5</sup>Department of Earth, Atmospheric and Planetary Sciences, Massachusetts Institute of Technology, Cambridge, MA 02139, USA

**Abstract**

New U–Pb radioisotopic ages on early Cambrian volcanic zircons condition a high-resolution Bayesian age model that constrains the first occurrences and zonations of West Gondwanan archaeocyaths and trilobites in southern Morocco. The oldest archaeocyaths in the Tiout Member of the Igoudine Formation (519.71 + 0.26/– 0.35 Ma) are *c.* 6 Ma younger than the oldest Siberian archaeocyaths. The oldest Moroccan trilobite fragments, from the lower member of the Igoudine, are constrained to 519.95 + 0.43/– 0.40 Ma. The succeeding Issendalenian Stage (i.e. *Hupetina antiqua* – *Eofallotaspis tioutensis* – *Fallotaspis plana* – *Choubertella* – *Daguinaspis* trilobite zones) spans *c.* 1.5 Ma (519.78 + 0.26/– 0.37 Ma to 518.43 + 0.25/– 0.69 Ma). Identifiable Moroccan fallotaspids and bigotinids, among Earth's oldest trilobites, occur above a positive  $\delta^{13}\text{C}$  excursion dated with our age model at 520.27 + 0.59/– 0.57 Ma, and correlated with the IV excursion peak *within* the lower range of Siberian Atdabanian Stage trilobites (*Repinaella* Zone). This excursion is the best standard for a Cambrian Series 2 base. The oldest West Gondwana trilobite fragments are *c.* 1 Ma younger than those in Siberia and *c.* 0.5 Ma older than the oldest Avalonian trilobites (*Callavia* Zone). This diachrony means a trilobite first appearance datum is an inappropriate chronostratigraphic base for Cambrian Series 2. Taxonomic differences in the oldest trilobites between Cambrian palaeocontinents are in accordance with trace fossil evidence for the group's appearance possibly as late as *c.* 530 Ma in the Cambrian Evolutionary Radiation. Coeval 519–517 Ma dates from Avalonia (cool-water siliciclastic shelf) and West Gondwana (tropical carbonate platform) sections with distinct macrofaunas emphasize these successions were latitudinally separate by the late Ediacaran Period.

**1. Introduction**

Development of a calibrated Cambrian timescale has resulted from precise U–Pb dating of volcanic ash zircons in fossiliferous marine successions (Landing *et al.* 1998; Harvey *et al.* 2011), combined with detailed carbon isotope chemostratigraphy (Kirschvink *et al.* 1991; Magaritz *et al.* 1991; Maloof *et al.* 2010). This work has led to a progressive stepwise ‘younging’ of the system and a shortening of the chronostratigraphic divisions of the Cambrian (e.g. Bowring & Schmitz, 2003, fig. 1; Peng *et al.* 2012). Precise U–Pb zircon dates also allow better estimates of rates of faunal turnover and oceanic geochemical changes (Maloof *et al.* 2005, 2010), the duration of biostratigraphic zones and the timing of geological events.

Radioisotopic ages and the marine record of carbon isotope excursions are particularly important for Cambrian correlation. Conventional biostratigraphic correlations are compromised by strong biogeographic, climate and lithofacies/habitat controls on the distributions of groups such as trilobites (which tend to be more offshore and unrestricted marine in distribution) and archaeocyaths (tropically restricted and which do not appear on cool-water palaeocontinents) (e.g. Debrenne & Debrenne, 1995; Landing & Westrop, 2004; Landing, 2005; Landing *et al.* 2013). In addition, regional unconformities of often undetermined duration, the problematical biostratigraphic utility of groups such as lower Cambrian acritarchs, and correlations of the upper lower Cambrian that are often based on genus- rather than species-level comparisons of trilobite faunas all work to confound precise interregional correlation (e.g. Landing *et al.* 2013). For these reasons, improved inter-palaeocontinent correlations must increasingly rely on highly precise U–Pb zircon dates and detailed geochemical stratigraphy,

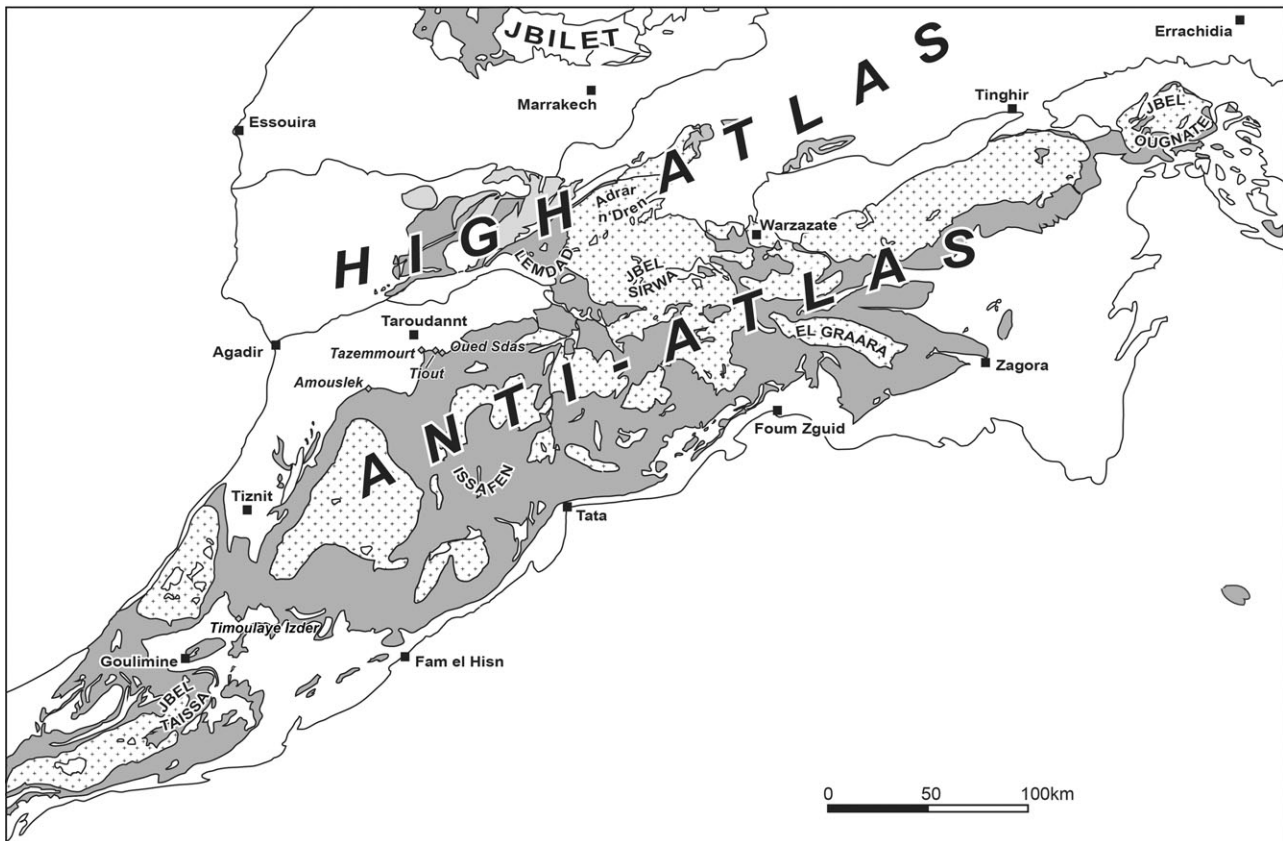


**Fig. 1.** Generalized geological map of southern Morocco showing Ediacaran–Cambrian rocks (medium grey), areas with Cambrian rocks (light grey) and outcrops of Neoproterozoic and Mesoproterozoic (Pan-African orogen, crosses). Trend of High Atlas and Anti-Atlas ranges shown and major basement massifs named (Adrar n'Dren, El Graara, Jbel Sirwa and Jbel Taïssa).

both of which must be calibrated against local biostratigraphic zonations (e.g. Landing *et al.* 1998; Maloof *et al.* 2010).

The fossil record of trilobites extends only as low as the upper lower Cambrian strata, *c.* 19 Ma after the beginning of the Cambrian Period (e.g. Landing *et al.* 1998; Landing, 1994; Peng & Babcock, 2005; Linnemann *et al.* 2019). Among the oldest of these are olenelloids of the superfamily Fallotaspidioidea Hupé, 1953b, which were first described and put into a biostratigraphic succession based on collections from the Tiout Member of the upper Igoudine Formation and overlying Amouslek Formation in southern Morocco (Figs 1, 2). This synthesis featured work by Neltner (1938), Neltner & Poctey (1950), Hupé & Abadie (1950) and, particularly, Hupé (1950, 1952, 1953a, b) (see reviews by Palmer & Repina, 1993; Geyer, 1996, 2019).

Collecting in western Laurentia (White-Inyo and Esmeralda mountains) and SW Siberia led to the recognition that the oldest trilobite faunas in these areas include taxa that were earlier identified as *Fallotaspis* Hupé, 1953b, and referred to a 'Fallotaspis Zone' that was compared with the lowest known Moroccan trilobite interval. Subsequent taxonomic work has referred the Siberian taxa to similar archaespind genera but affirmed the presence of *Fallotaspis*, or a genus very similar to *Fallotaspis*, in the White-Inyo Mountains of California and western Nevada (reviews in Geyer, 1996; Hollingsworth, 2007; Landing *et al.* 2013).

With fallotaspids regarded as keys to early trilobite evolution and global correlation, the well-exposed section at Tiout, southern Morocco (Fig. 1), has become particularly important. Sdzuy (1978)

described horizons with fallotaspid and bigotinid trilobites at the Tiout section. A recent comprehensive study of these earliest trilobites from Tiout and comparable sections at Tazemmourt and Amouslek (Geyer, 2019) shows that numerous taxa of the Bigotinidae and Fallotaspididae occur in the Tiout Member of Geyer (1990), down to a level with the lowest known identifiable Moroccan trilobites (Fig. 3, 'T'-horizons). These trilobites are complemented by the oldest archaeocyath-bearing beds (Fig. 3, 'A'-horizons) known in Morocco and West Gondwana (Debrenne & Debrenne, 1978, 1995; Debrenne *et al.* 1992).

As work much lower in the Tiout section recorded datable volcanic ashes in the Lie de vin Formation (Monninger, 1979; Compston *et al.* 1992; Landing *et al.* 1998; Fig. 2), it was our belief that higher volcanic ashes occurred and that U–Pb dating using modern chemical abrasion isotope dilution thermal ionization mass spectrometry (CA-ID-TIMS) protocols could yield refined geochronologic brackets on the oldest Moroccan trilobites and archaeocyaths. It is important to emphasize 'identifiable trilobites', as fragmentary sclerites occur *c.* 30 m below the Tiout Member of the Igoudine Formation at Tiout (Geyer & Landing, 1995, 2006b; Geyer, 2019). This report also includes a reanalysis of the U–Pb zircon age on a sample in the Lie de vin Formation (Tiout 566 of Landing *et al.* 1998) below these lowest known trilobite fragments. The five new U–Pb ages reported here are combined within a Bayesian statistical framework to build a robust age model for these earliest trilobites and archaeocyaths, and the associated carbon isotope stratigraphy.

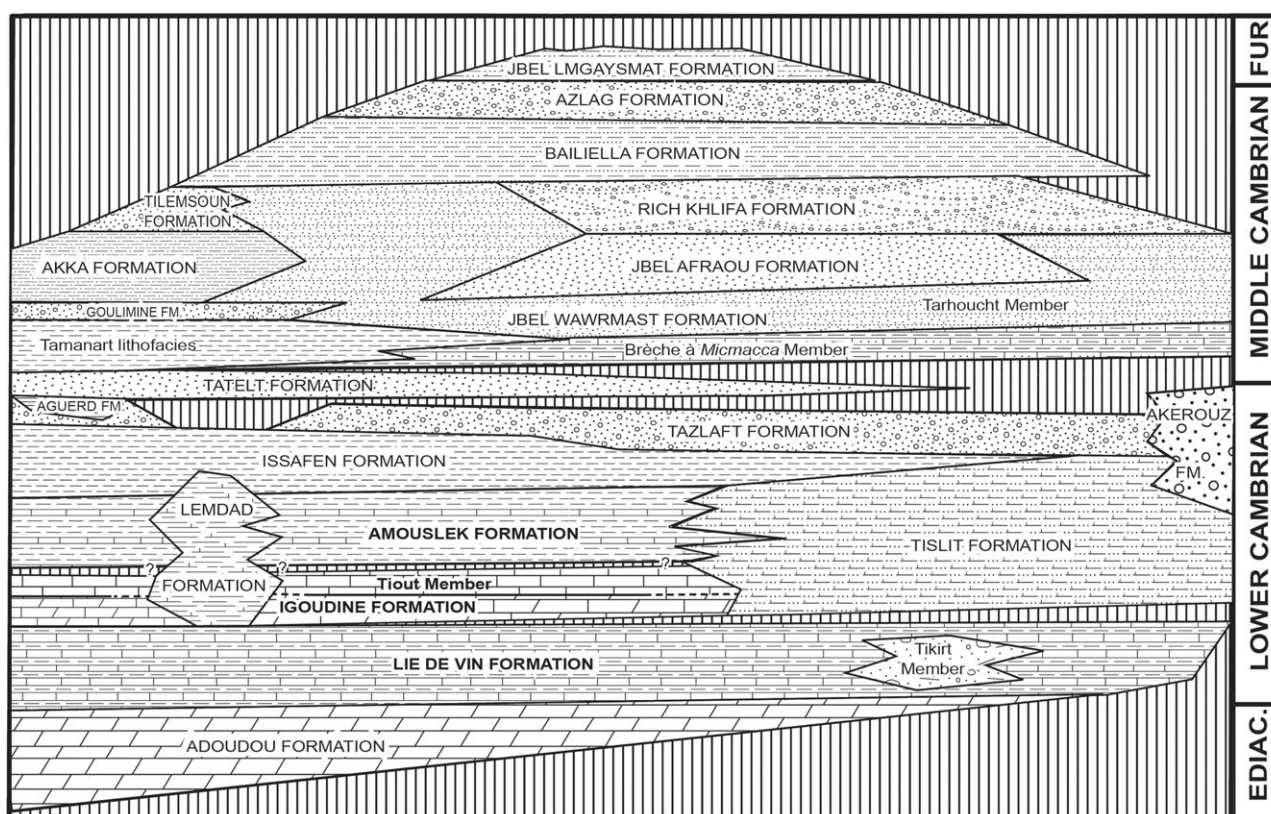


**Fig. 2.** Terminal Ediacaran–Cambrian lithostratigraphic units of the Moroccan Atlas regions; cross-section runs west (right-hand side) to east (left) and includes Lemdad Formation facies of the High Atlas; vertical lines indicate unconformity. Regional extent of sequence boundary at Igoudine–Amouslek Formation contact at Tiout unknown. Figure modified from Geyer & Landing (2006a, fig. 2), using traditional lower and middle Cambrian subdivisions. Lower–middle Cambrian boundary interval regressive, macrotidal sandstones of Tazlaft Formation distinguished from unconformably overlying, volcanic-rich, wave-dominated sandstones of Talelt Formation, which unconformably locally overlies units as low as the Issafen Formation (Landing *et al.* 2006). The succession of the regressive Tazlaft–overlying transensional Talelt depositional sequence is readily distinguished for c. 200 km in the Anti-Atlas and High Atlas ranges; the units must not be combined into a single unit and mapped as the traditional ‘regressive’ Asrir Formation (e.g. Alvaro *et al.* 2014).

## 2. Geology

### 2.a. Generalized setting

The rock successions of the Atlas ranges include early Ediacaran andesites, rhyolites and ignimbrites with 565–560 Ma dates at their tops (e.g. Mifdal & Peucat, 1985; Walsh *et al.* 2002; Maloof *et al.* 2005) that overlie Meso- and Neoproterozoic rocks of the Pan-African orogen (Fig. 1). These older units are unconformably overlain by the marine-dominated cover sequence of the terminal Ediacaran–Silurian Sous Basin (Geyer, 1989), which roughly parallels the trend of the Anti-Atlas.

### 2.b. Adoudou Formation

The initial deposits of this cover sequence (Fig. 2) form the Adoudou Formation (Geyer, 1989). This unit was divided by Maloof *et al.* (2005) into a lower Tabia Member (0–250 m of lower coarse siliciclastics with massive conglomerate; middle evaporitic dolostone and limestone; and an upper shale-dominated, heterolithic interval with conglomerate, arkose, sandstone and carbonate) and an upper Tifnout Member (up to 1000 m of shallow-marine, massive carbonate and minor siliciclastic beds with desiccation and tepee structures and gypsum moulds; see Monninger, 1979). Fossils, except for stromatolites and poorly preserved ichnofossils, are unknown in the Adoudou Formation.

Correlation of the Adoudou Formation is based on a  $-6\text{‰}$   $\delta^{13}\text{C}$  nadir in the lower Tifnout Member that is regarded as marking the

Ediacaran–Cambrian boundary (Maloof *et al.* 2005, fig. 2, but also reported as at the ‘base of the Tifnout’ on p. 2206). The middle Tifnout Member at Oued Sdas, c. 5.0 km east of the Tiout section, has a tuff with a weighted mean zircon  $^{206}\text{Pb}/^{238}\text{U}$  age of  $525.23 \pm 0.12$  (0.38) [0.94] Ma (Maloof *et al.* 2010, fig. 2). This tuff is likely correlative, in part, with the Tommotian Stage of the Siberian Platform (Maloof *et al.* 2010) and upper Stage 2 of the global lowest Cambrian chronostratigraphic reference section (see Terreneuvian Series geochronology in Landing & Kouchinsky, 2016).

### 2.c. Lie de vin Formation

Continued restricted marine deposition is recorded by cyclically bedded siltstone and carbonate of the Lie de vin Formation (Choubert, 1952; to 940 m thick at Tiout), with rare stromatolites, thrombolites and evaporite mineral pseudomorphs (Monninger, 1979). The Lie de vin has Cambrian-aspect trace fossils (e.g. a form identified as *Diplocraterion* in Latham & Riding, 1990, fig. 2). An early Cambrian SHRIMP U–Pb zircon date of  $521 \pm 7$  Ma was determined 730 m above the base of the Lie de vin Formation (Compston *et al.* 1992), with a more refined ID-TIMS U–Pb zircon date of  $522 \pm 2$  Ma at 763 m at the Tiout section (Landing *et al.* 1998). Maloof *et al.* (2010) reported a CA-ID-TIMS U–Pb zircon date of  $520.93 \pm 0.14$  Ma for a tuff in the upper Lie de vin Formation at 1736 m in the Oued Sdas section, purportedly near the same stratigraphic level as the coeval date

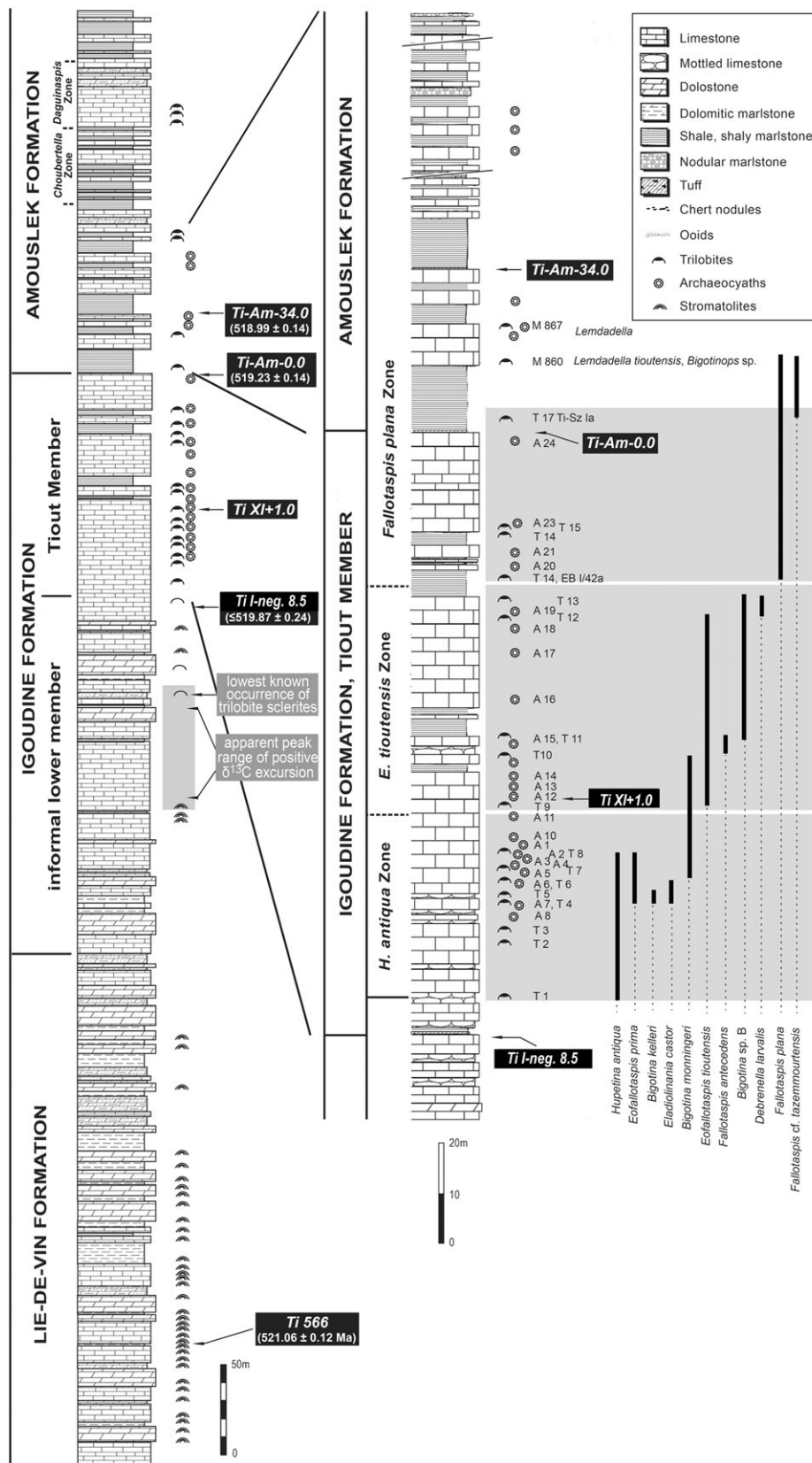


**Fig. 3.** Upper Igoudine (and Tiout Member) – lower Amouslek Formation at the Tiout section shows ashes and volcaniclastic sandstones examined in this study (Ti-I-neg8.5, Ti-XI-1.0, Ti-Am-0.0, Ti-Am-34.0). Horizons in Tiout Member with trilobites (Sdzuy, 1978) have the prefix ‘T’; archaeocyathan horizons (partly also with determinable trilobites) (Debrene & Debrene, 1978, 1995; Debrene et al. 1992) have the prefix ‘A’. Selected trilobite ranges from Geyer (2019). Section modified from Sdzuy (1978, fig. 2b) and Schmitt (1979, fig. 44).

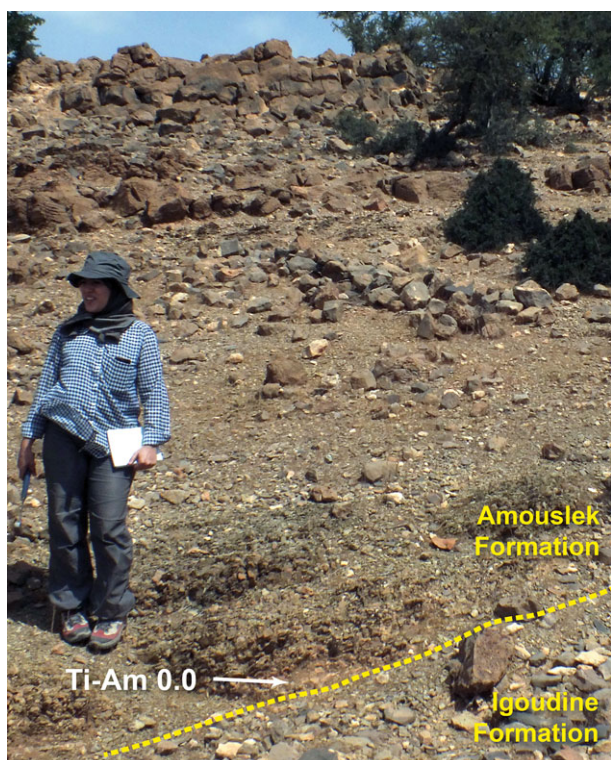


**Fig. 4.** (Colour online) Volcanic ash at base of Amouslek Formation mantles sequence boundary on the Tiout Member of the upper Igoudine Formation at Tiout.

in the Tiout section (Fig. 1). These dates are broadly consistent with proposed  $\delta^{13}\text{C}$  correlations of the Lie de vin Formation with the Siberian Tommotian Stage (e.g. Brasier *et al.* 1991; Magaritz *et al.* 1991; Maloof *et al.* 2005).

Boudda & Choubert (1972) reported trilobite fragments from rocks assigned to the upper Lie de vin Formation in the High Atlas range. However, these undescribed fragments actually come from a red siliciclastic mudstone in the lowest Lemdad Formation (Fig. 2) that is now correlated with the lower Igoudine Formation (Sdzuy, 1978; Geyer & Landing, 2006b, p. 72). Unidentified trilobite fragments also occur in the lower Igoudine Formation at the Tiout section in the Anti-Atlas (Geyer & Landing, 1995, p. 35, 2006b), providing a compelling reason to refine the U–Pb zircon date on an ash (Tiout 566) 180 m below the top of the Lie de vin (Monninger, 1979; Landing *et al.* 1998) in order to bracket the lowest local occurrence, and perhaps global appearance, of trilobites.

#### 2.d. Igoudine and Amouslek formations

The highest units in this report are the Igoudine and Amouslek formations of Geyer (1989; Fig. 2). Development of an extensive carbonate platform following regional marine deepening is recorded by the massive, dove-grey weathering, black limestone-dominated Igoudine Formation (up to 400 m thick, with c. 190 m at the Tiout section; Monninger, 1979).

Further deepening is recorded by the change from an unnamed lower member of the Igoudine Formation, with black laminated limestones and dolosiltites and unidentifiable trilobite sclerites (Geyer & Landing, 1995, 2006a, b), into the fossiliferous Tiout Member (Geyer, 1989) of the upper Igoudine (Figs 2, 3). The overlying Amouslek Formation represents open-marine deposition with abundant trilobites and archaeocyaths. This unit (260 m at Tiout; Monninger, 1979) features a distinctive change

from massive carbonates of the Igoudine Formation up into initially siliciclastic mudstone-dominated deposits of the Amouslek Formation. The Igoudine–Amouslek contact is an unconformity mantled with an ash (Geyer & Landing, 2006a, b; sample Ti-Am-0.0 here), which is best regarded as a sequence boundary in the Anti-Atlas (Figs 2, 4). The gradual upwards increase in carbonate beds through the formation makes the Amouslek comparable to a ‘Grand cycle’, as first described in west Laurentia (Geyer & Landing, 1995).

#### 2.e. Tiout Member

The Tiout Member has ooid pack- and wackestones and an abundant macrofauna with identifiable trilobites, archaeocyaths, hyoliths and cancelloriids. The stratigraphically abrupt appearances of trilobites and, 13 m higher, of the oldest Moroccan archaeocyaths at the Tiout section (Figs 1, 3) do not reflect evolutionary events but track the appearance of more normal marine facies (Monninger, 1979; Geyer, 1989; Geyer & Landing, 1995; Landing *et al.* 2013). Sdzuy’s (1978) work, which established the *Eofallotaspis* Zone, documented the lowest known identifiable trilobites in Morocco, with rare trilobite fragments found low in the lower member of the Igoudine Formation (Fig. 2) (Geyer & Landing, 1995, 2006b).

#### 2.f. Tiout and Timoulaye Izder sections

The N-dipping (25–35°) Tiout section lies at the north rim of the Anti-Atlas and about 25 km SE of Taroudant (Fig. 1). This is certainly the best studied and referenced Cambrian succession in Morocco. It extends along a canyon from the poorly exposed Tabia Member of the Adoudou Formation (at a hamlet at c. 30° 20′ 30″ N, 8° 41′ 50″ W) through the lower 260 m of the Amouslek Formation (Geyer & Landing, 1995, 2006b; see Stop 1 of both field guides). The upper, most relevant part of the section lies at c. 30° 22′ 40″ N, 8° 41′ 20″ W. Monninger (1979) measured the Tiout section beginning in the upper 200 m of the Adoudou Formation. He painted numbers on each of his described beds through the Igoudine Formation that are still visible at places as an aid in field work. The early Cambrian U–Pb zircon dates from the Lie de vin Formation described above (Section 2.c) come from his beds 563 and 566 on the east side of the canyon.

The upper part of the lower member of the Igoudine Formation and the Tiout Member are exposed high in the cliffs on the east side of the canyon mouth at Tiout. Some of the horizons that yielded trilobites and archaeocyaths from the Tiout Member in the 1970s are painted with a letter–number designation. Each of the fossiliferous horizons in Figure 3 can therefore be readily located (although the markings have decayed over the last decade). These fossils include Sdzuy’s (1978) trilobite horizons T1–T17, and the oldest known Moroccan archaeocyath-bearing levels at horizons A1–A24 of Debrenne & Debrenne (1978, 1995) and Debrenne *et al.* (1992). Some archaeocyath horizons also yield trilobites (Fig. 3).

The Timoulaye Izder section is c. 2 km NE of Timoulaye Izder village on the NW margin of the Anti-Atlas (Fig. 1; c. 20° 12′ 30″ N, 9° 35′ 50″ W). It exposes the upper Igoudine (Tiout Member) through middle Issafen formations in a lithofacies different from that in the Tiout section, but characteristic of the western Anti-Atlas (Geyer & Landing, 2006b). The succession progressively steepens in dip from 20–27° SE on the cliff-forming Tiout Member – Amouslek Formation to nearly vertical on the slope-forming Issafen Formation. A total of 27 m of

brownish-weathering Tiout Member are exposed on the dip slope, and are succeeded by a thick (27–312 m), deepening–shoaling succession through the Amouslek. The lowest Amouslek is nodular, trilobite-bearing wackestones in green shale, and the lower Amouslek is dominated by massive, algal build-ups (Geyer & Landing, 2006b). The middle Amouslek (79.5–288 m) is dominantly deeper-water, trilobite-bearing, bluish green to green siltstone and shale with thin nodular and trilobite hash limestone. Shallowing is obvious in the uppermost Amouslek, with evidence for shallow-water, wave-dominated deposition of fine-quartz sand- and ooid/pisolite-dominated intervals, and increased rates of deposition suggested by ball-and-pillow structures (Geyer & Landing, 2006b). Sample Tim-269.5 comes from the upper Amouslek Formation at the Timoulaye Izder section, within the upper *Choubertella*, or possibly the lower *Daguinaspis* Zone (G. Geyer, unpublished data).

### 2.g. Tiout faunas and an emended biostratigraphy

All of the trilobite-bearing horizons in the Tiout Member at Tiout (Fig. 1) were referred to the ‘*Eofallotaspis* beds’ by Sdzuy (1978) and subsequently termed the ‘*Eofallotaspis* Zone’ (Geyer, 1990). These trilobite assemblages were initially believed to show little difference in faunal composition through c. 110 m of the Tiout Member (Geyer & Landing, 1995, 2006b) and thought to reflect a relatively brief geological interval. A recent study by Geyer (2019) shows a very rapid vertical change in trilobite faunas and their diversity in the Tiout Member and lower Amouslek Formation. This required division of the *Eofallotaspis* Zone of Sdzuy (1978) into a lower *Hupetina antiqua* and an upper *Eofallotaspis tioutensis* Zone, as well as modification of the overlying, previously defined *Fallotaspis tazemmourtensis* Zone to a new *Fallotaspis plana* Zone with a slightly lower lower boundary. The lowest known *Fallotaspis plana* at horizon T14 is used to assign the upper range of *E. tioutensis* to the *F. plana* Zone. Hupé’s (1952, 1953a) and Geyer’s (1990) original *F. tazemmourtensis* Zone was earlier recognized as a thin and likely temporally brief interval at other sections (e.g. Tazemmourt; Geyer, 1996) equivalent to the upper *F. plana* Zone.

Bigotiniids dominate the trilobites through the Tiout Member, and *Eofallotaspis* persists through much of the Tiout (Geyer, 2019). All trilobites of these surprisingly diverse associations belong to the Bigotiniidae and Fallotaspidae, of which only *Hupetina antiqua*, *Eofallotaspis prima*, *E. tioutensis* and *Fallotaspis* cf. *F. tazemmourtensis* were earlier identified by Sdzuy (1978, 1981). Geyer (2019) introduced the new genera and species *Bigotina kelleri*, *B. monningeri*, *Issendalenia grandispina*, *Tioutella floccofavosa*, *Pseudobigotina antiatlasensis*, *Eladiolinania castor*, *E. pollux*, *Debrenella larvalis* and *Fallotaspis antecessens* from the Tiout section, and *Bigotinops chouberti* from below the known range of *F. tazemmourtensis* in the Amouslek section.

The successive higher zones named by Hupé (1953a) (*Fallotaspis tazemmourtensis*, *Choubertella* and *Daguinaspis* zones) in southern Morocco were based on the lowest occurrences of the eponymous fallotaspidoid genera and species. The recovery of *F. cf. tazemmourtensis* Hupé, 1953a and *F. plana* below the Amouslek Formation, and thus a range overlapping with that of *Eofallotaspis* spp., required a change of the biostratigraphical concepts and the zonal boundaries (Geyer, 2019; Fig. 3).

*Fallotaspis tazemmourtensis* and *F. plana* appear to be limited to shaly rocks (Geyer, 1996, 2019), with the lowest occurrence of the species in a shaly layer in the Tiout Member at Tiout (Fig. 3,

horizon T14). However, an even earlier species of *Fallotaspis*, *F. antecessens* Geyer, 2019, also occurs in limestones (Fig. 3).

Biostratigraphic re-evaluation of the Tiout section also included the fact that sclerites tentatively attributed to *Fallotaspis bondoni* (Neltner & Poctey, 1950) are now known near the base of the c. 260-m-thick overlying Amouslek Formation (Fig. 3). Other occurrences of *F. bondoni* are limited to the Amouslek Formation above the *Fallotaspis plana* Zone and are from the higher *Choubertella* and *Daguinaspis* zones in southern Morocco (Geyer, 1996). Probable recovery of *F. bondoni* at Tiout suggests that the lower Amouslek Formation probably belongs to the *Choubertella* Zone (Fig. 3). *Daguinaspis* (the index fossil of the zone above the *Choubertella* Zone) is a frequent faunal element in the upper–uppermost Amouslek and occurs only higher in the Amouslek at Tiout (Geyer, 1996; Geyer & Landing, 2006b, p. 53). It should be noted, however, that *Lemdadella tioutensis* and *Bigotinops* sp. occur in the Tiout section in the lowest limestone of the Amouslek Formation and above the shales with *F. cf. bondoni*. *Lemdadella tioutensis* was described by Sdzuy (in Liñán & Sdzuy, 1978) from Tiout and assigned to Hupé’s (1953a) *F. tazemmourtensis* Zone, although neither *F. tazemmourtensis* (from sample TIOU-T14) nor *F. cf. bondoni* (from TI-Sz Ia) were known at that time from Tiout (samples in Geyer & Landing, 1995, p. 59).

The *Hupetina antiqua* – *Eofallotaspis tioutensis* succession is complemented by numerous horizons with archaeocyaths, with a lowest appearance of determinable archaeocyaths 13 m above the lowest identifiable trilobites (Debrenne & Debrenne, 1978; Debrenne et al. 1992) and above the lithofacies change from the lower Igoudine Formation into the Tiout Member. A lowest archaeocyath zone (*Erismacoscinus fasciola* – *Retecoscinus minutus* Zone) is recognized through the Tiout Member and equated with the *Eofallotaspis* beds and Zone of Sdzuy (1978) and Geyer (1990) (Debrenne & Debrenne, 1978, 1995). The two eponymous species of the oldest archaeocyath zone do not appear above the Tiout Member. The overlying Amouslek Formation brackets the long-ranging *Erismacoscinus maroccanus* Zone and the traditional *Fallotaspis tazemmourtensis* (extended downwards in this report to horizon T14), *Choubertella* and *Daguinaspis* trilobite zones (e.g. Debrenne & Debrenne, 1995, p. 122). It should be noted that, in contrast to the trilobite succession, no significant change in composition of the archaeocyath assemblages can be recognized in the Tiout Member.

The *Hupetina antiqua* through *Daguinaspis* zonal succession is significant as it defines the Issendalenian Stage low in the lower Cambrian strata of the West Gondwanan composite chronostratigraphic succession. It is equivalent to most of the traditional ‘Ovetian Stage’ of Iberia (Geyer & Landing, 2004).

## 3. Methods

### 3.a. U–Pb geochronology

The dove-grey weathering, black limestones of the upper Igoudine Formation (Tiout Member) at Tiout contain a small number of brown weathering, thin siliciclastic sandstones. Two of these with high feldspar content and potential volcanic lapilli fragments were sampled (Ti-I-neg8.5 and Ti-XI+1). Fine-grained volcanic tuffs were also sampled at the base of the Amouslek Formation (Ti-Am-0.0) and higher in the formation (Ti-Am-34.0). The tuff at 763 m (Section 2.c) in the Tiout section (Ti-566) was re-dated

in this study from the same mineral separation prepared and reported by Landing *et al.* (1998).

Zircon crystals were separated from hand samples by conventional density and magnetic methods (Table 1). The entire zircon separate was placed in a muffle furnace at 900°C for 60 hours in quartz beakers to anneal minor radiation damage; annealing enhances cathodoluminescence emission (Nasdala *et al.* 2002), promotes more reproducible inter-element fractionation during laser ablation inductively coupled plasma mass spectrometry (LA-ICP-MS) (Allen & Campbell, 2012), and prepares the crystals for subsequent chemical abrasion (Mattinson, 2005). Following annealing, individual grains were hand-picked and mounted, polished and imaged by cathodoluminescence (CL) on a scanning electron microscope. From these compiled images, grains with consistent and dominant CL patterns were selected for further isotopic analysis.

The methods for U–Pb geochronology by both LA-ICP-MS and CA-ID-TIMS follow those of Schmitz & Davydov (2012) and MacDonald *et al.* (2018). A full suite of trace-element concentrations in zircon, as well as low-resolution U–Pb dates, were obtained by LA-ICP-MS on 25 µm diameter spot domains on multiple zircon crystals for each sample (online Supplementary Tables S1–S3, available at <http://journals.cambridge.org/geo>). Blank-subtracted trace-element analyte signals were internally normalized to <sup>29</sup>Si and calibrated to NIST-610 and -612 glasses. U–Pb and Pb–Pb dates were calibrated with respect to interspersed measurements of several zircon reference materials. The primary standard Plešovice zircon (Sláma *et al.* 2008) was used to monitor time-dependent instrumental fractionation, and a secondary correction was subsequently applied to each analysis as a function of radiogenic Pb count rate compared with the returned age bias in reference materials including Seiland, Zirconia and Plešovice zircon.

Following LA-ICP-MS spot analysis, selected zircon crystals were subjected to a modified version of the chemical abrasion method of Mattinson (2005), whereby single crystal fragments plucked from grain mounts were individually abraded in a single step with concentrated hydrogen fluoride at 180°C for 12 hours. Residual crystals were rinsed, spiked with the ET535 mixed <sup>205</sup>Pb–<sup>233</sup>U–<sup>235</sup>U tracer solution, and processed for ID-TIMS analysis. U–Pb dates and uncertainties for each CA-ID-TIMS analysis were calculated using the algorithms of Schmitz & Schoene (2007) and the U decay constants of Jaffey *et al.* (1971). Uncertainties are based upon non-systematic analytical errors, including counting statistics, instrumental fractionation, tracer subtraction and blank subtraction. These error estimates should be considered when comparing our <sup>206</sup>Pb/<sup>238</sup>U dates with those from other laboratories that used tracer solutions calibrated against the EARTHTIME gravimetric standards. When comparing our dates with those derived from other decay schemes (e.g. <sup>40</sup>Ar/<sup>39</sup>Ar, <sup>187</sup>Re–<sup>187</sup>Os), the uncertainties in tracer calibration (0.03%; Condon *et al.* 2015; McLean *et al.* 2015) and U decay constants (0.108%; Jaffey *et al.* 1971) should be added to the internal error in quadrature. Quoted errors for calculated weighted means are therefore of the form ±X(Y)[Z], where X is solely analytical uncertainty, Y is the combined analytical and tracer uncertainty, and Z is the combined analytical, tracer and <sup>238</sup>U decay constant uncertainty. The mean squared weighted deviation (MSWD; Wendt & Carl, 1991) was used to evaluate the goodness of fit of weighted mean model ages (online Supplementary Files S1–S4, available at <http://journals.cambridge.org/geo>).

### 3.b. Bayesian age modelling

Bayesian models attempt to estimate the probable values of unknown parameters ( $\theta$ ) based on prior information about these parameters, which can be conditioned by observed data, or likelihoods ( $x$ ). In the case of age modelling, dated horizons at particular stratigraphic levels ( $x$ ) condition the parameters of the age model ( $\theta$ ) in concert with prior knowledge of those parameters from constraints such as stratigraphic superposition and/or assumptions of sedimentation rate and its variability. We used the Bayesian age modelling software modifiedBchron (Trayler *et al.* 2019), an open-source R package evolved from the package Bchron (Haslett & Parnell, 2008) for deep time applications. These packages are identical in their use of a compound Poisson-gamma distribution of accumulation events under the constraint of stratigraphic superposition to describe the prior probability of an ensemble of piece-wise linear sedimentation paths, which are conditioned by likelihood functions describing dated horizons (Haslett & Parnell, 2008). Additionally, modifiedBchron uses an adaptive proposal algorithm in its Markov Chain Monte Carlo engine to remove any necessity for user scaling of the space or time domains, and still ensure effective and efficient sampling of the posterior parameter distributions (Trayler *et al.* 2019). For the likelihood functions, modifiedBchron can represent radioisotopic ages as a single Gaussian normal distribution (e.g. to represent a weighted mean age), but can also aggregate individual (normally distributed) crystal analyses of a sample at a given stratigraphic horizon to accurately reflect the complex probability function of dated crystals in some volcanic event beds. Similarly, uniform distributions can be input as likelihood functions (e.g. to represent magnetostratigraphic, chemostratigraphic or cyclostratigraphic signals), and aggregated at any stratigraphic horizon to approximate any arbitrarily complex distribution (e.g. arising from detrital zircon maximum depositional age constraints).

## 4. Results

### 4.a. Tiout 566

As part of this study, the age of the 10-cm-thick ash collected at 763 m in the Tiout section and reported as 522 ± 2 Ma (Landing *et al.* 1998, their sample Tiout 566) was re-measured using chemical abrasion TIMS methods. This sample is *c.* 210 m below the top of the Lie de vin Formation and *c.* 310 m below the carbon excursion in the lower member of the Igoudine Formation that is equated with the Siberian IV excursion. Sample Tiout 566 is 500 m below the base of the Tiout Member with its trilobites and archaeocyaths (Monninger, 1979; Kirschvink *et al.* 1991).

Cathodoluminescence imaging of mounted zircons revealed a bimodal distribution of CL-dark, oscillatory zoned crystals and CL-bright weakly zoned crystals (online Supplementary Fig. S1, available at <http://journals.cambridge.org/geo>). LA-ICP-MS spot analyses produced a majority of Cambrian and a minority of late Ediacaran <sup>206</sup>Pb/<sup>238</sup>U dates, irrespective of CL pattern. Trace-element concentrations and ratios for these zircons are plotted in Figure 5; the Tiout 566 zircon compositions define two fields or branches in bivariate and ternary spaces. Seven crystals chosen from both subpopulations were selected for CA-ID-TIMS analysis; all seven crystals yielded concordant and equivalent U–Pb dates, with a weighted mean <sup>206</sup>Pb/<sup>238</sup>U date of 521.06 ± 0.12 (0.28) [0.61] Ma (MSWD = 0.61; Fig. 6). The invariance in age as a function of zoning and composition is taken as

**Table 1.** Zircon chemical abrasion IDTIMS U-Pb isotopic data

| Grain<br>(a)  | Th/U<br>(b)  | <sup>206</sup> Pb* × 10 <sup>-13</sup><br>(c) | mol %<br>(c) | <sup>206</sup> Pb*<br>(c) | Pb*/Pbc<br>(c) | Pbc (pg)<br>(c) | <sup>206</sup> Pb/ <sup>204</sup> Pb<br>(d) | Radiogenic isotopic ratios                  |   |                 |  |                 |  | Corr. coeff.<br>(f) | Radiogenic isotopic dates |   |  |  |               |             |  |
|---|--------------|---|--------------|---------------------------|----------------|-----------------|---|---|---|-----------------|--|-----------------|--|---------------------|---------------------------|---|--|--|---------------|-------------|--|
|   |              |   |              |                           |                |                 |   | <sup>208</sup> Pb/ <sup>206</sup> Pb<br>(e) | <sup>207</sup> Pb/ <sup>206</sup> Pb<br>(e) | % Error<br>(f)  | <sup>207</sup> Pb/ <sup>235</sup> U<br>(e) | % Error<br>(f)  | <sup>206</sup> Pb/ <sup>238</sup> U<br>(e) |                     | % Error<br>(f)            | <sup>207</sup> Pb/ <sup>206</sup> Pb ±<br>(g) | <sup>207</sup> Pb/ <sup>235</sup> U ±<br>(g) | <sup>206</sup> Pb/ <sup>238</sup> U ±<br>(g) | ±<br>(f)      |             |  |
| <b>Tim-269.5</b>  |              |   |              |                           |                |                 |   |   |   |                 |  |                 |  |                     |                           |   |  |  |               |             |  |
| z1  | 0.532        | 0.8231  | 99.66        | 89                        | 0.23           | 5264            | 0.166                                       | 0.06000                                     | 0.111                                       | 0.811438        | 0.164                                      | 0.098086        | 0.072                                      | 0.836               | 603.6                     | 2.4   | 603.26                                       | 0.74   | 603.18        | 0.41        |  |
| z8  | 0.280        | 0.5602  | 99.38        | 45                        | 0.29           | 2890            | 0.087                                       | 0.05900                                     | 0.190                                       | 0.748576        | 0.241                                      | 0.092026        | 0.094                                      | 0.680               | 567.0                     | 4.1   | 567.40                                       | 1.05   | 567.51        | 0.51        |  |
| z5  | 0.398        | 2.5500  | 99.87        | 222                       | 0.28           | 13652           | 0.124                                       | 0.05910                                     | 0.070                                       | 0.749692        | 0.132                                      | 0.092010        | 0.069                                      | 0.949               | 570.6                     | 1.5   | 568.05                                       | 0.58   | 567.41        | 0.38        |  |
| z6  | 0.287        | 0.2693  | 98.50        | 19                        | 0.34           | 1202            | 0.089                                       | 0.05891                                     | 0.425                                       | 0.741664        | 0.544                                      | 0.091312        | 0.265                                      | 0.644               | 563.7                     | 9.3   | 563.38                                       | 2.35   | 563.29        | 1.43        |  |
| z7  | 0.277        | 0.2688  | 99.26        | 38                        | 0.17           | 2429            | 0.086                                       | 0.05787                                     | 0.248                                       | 0.673788        | 0.295                                      | 0.084450        | 0.093                                      | 0.620               | 524.7                     | 5.5   | 523.01                                       | 1.21   | 522.63        | 0.47        |  |
| <b>z2</b>   | <b>0.426</b> | <b>1.1189</b>                                 | <b>99.35</b> | <b>45</b>                 | <b>0.61</b>    | <b>2757</b>     | <b>0.133</b>                                | <b>0.05786</b>                              | <b>0.153</b>                                | <b>0.668405</b> | <b>0.199</b>                               | <b>0.083787</b> | <b>0.069</b>                               | <b>0.756</b>        | <b>524.4</b>              | <b>3.4</b>                                    | <b>519.74</b>                                | <b>0.81</b>                                  | <b>518.69</b> | <b>0.34</b> |  |
| <b>z3</b>   | <b>0.518</b> | <b>0.8553</b>                                 | <b>98.34</b> | <b>18</b>                 | <b>1.21</b>    | <b>1076</b>     | <b>0.162</b>                                | <b>0.05772</b>                              | <b>0.204</b>                                | <b>0.666613</b> | <b>0.253</b>                               | <b>0.083764</b> | <b>0.072</b>                               | <b>0.759</b>        | <b>519.1</b>              | <b>4.5</b>                                    | <b>518.65</b>                                | <b>1.03</b>                                  | <b>518.55</b> | <b>0.36</b> |  |
| <b>z4</b>   | <b>0.391</b> | <b>0.9953</b>                                 | <b>99.71</b> | <b>100</b>                | <b>0.24</b>    | <b>6145</b>     | <b>0.122</b>                                | <b>0.05776</b>                              | <b>0.097</b>                                | <b>0.667069</b> | <b>0.152</b>                               | <b>0.083762</b> | <b>0.070</b>                               | <b>0.878</b>        | <b>520.6</b>              | <b>2.1</b>                                    | <b>518.93</b>                                | <b>0.62</b>                                  | <b>518.54</b> | <b>0.35</b> |  |
| Weighted mean <sup>206</sup> Pb/ <sup>238</sup> U age = 518.59 ± 0.20 (0.32) [0.63] Ma (2 s); MSWD = 0.22 (n = 3) (h) |              |   |              |                           |                |                 |   |   |   |                 |  |                 |  |                     |                           |   |  |  |               |             |  |
| <b>Ti-Am-34.0</b>   |              |   |              |                           |                |                 |   |   |   |                 |  |                 |  |                     |                           |   |  |  |               |             |  |
| z8  | 0.219        | 0.652   | 99.2         | 33                        | 0.46           | 2128            | 0.069                                       | 0.05781                                     | 0.204                                       | 0.66939         | 0.252                                      | 0.083984        | 0.085                                      | 0.684               | 522.5                     | 4.5   | 520.34                                       | 1.03   | 519.86        | 0.42        |  |
| <b>z3</b>   | <b>0.236</b> | <b>2.717</b>                                  | <b>99.7</b>  | <b>105</b>                | <b>0.61</b>    | <b>6723</b>     | <b>0.074</b>                                | <b>0.05779</b>                              | <b>0.080</b>                                | <b>0.66827</b>  | <b>0.139</b>                               | <b>0.083866</b> | <b>0.066</b>                               | <b>0.939</b>        | <b>521.9</b>              | <b>1.7</b>                                    | <b>519.66</b>                                | <b>0.56</b>                                  | <b>519.16</b> | <b>0.33</b> |  |
| <b>z1</b>   | <b>0.251</b> | <b>3.805</b>                                  | <b>99.9</b>  | <b>283</b>                | <b>0.32</b>    | <b>18089</b>    | <b>0.079</b>                                | <b>0.05778</b>                              | <b>0.060</b>                                | <b>0.66804</b>  | <b>0.124</b>                               | <b>0.083851</b> | <b>0.064</b>                               | <b>0.997</b>        | <b>521.5</b>              | <b>1.3</b>                                    | <b>519.52</b>                                | <b>0.51</b>                                  | <b>519.07</b> | <b>0.32</b> |  |
| <b>z7</b>   | <b>0.209</b> | <b>0.719</b>                                  | <b>99.3</b>  | <b>39</b>                 | <b>0.43</b>    | <b>2541</b>     | <b>0.065</b>                                | <b>0.05780</b>                              | <b>0.164</b>                                | <b>0.66806</b>  | <b>0.210</b>                               | <b>0.083831</b> | <b>0.070</b>                               | <b>0.757</b>        | <b>522.1</b>              | <b>3.6</b>                                    | <b>519.53</b>                                | <b>0.85</b>                                  | <b>518.95</b> | <b>0.35</b> |  |
| <b>z2</b>   | <b>0.214</b> | <b>2.203</b>                                  | <b>99.8</b>  | <b>132</b>                | <b>0.39</b>    | <b>8549</b>     | <b>0.067</b>                                | <b>0.05774</b>                              | <b>0.145</b>                                | <b>0.66739</b>  | <b>0.183</b>                               | <b>0.083825</b> | <b>0.077</b>                               | <b>0.658</b>        | <b>520.0</b>              | <b>3.2</b>                                    | <b>519.12</b>                                | <b>0.74</b>                                  | <b>518.91</b> | <b>0.38</b> |  |
| <b>z5</b>   | <b>0.377</b> | <b>0.697</b>                                  | <b>99.5</b>  | <b>57</b>                 | <b>0.29</b>    | <b>3558</b>     | <b>0.118</b>                                | <b>0.05773</b>                              | <b>0.158</b>                                | <b>0.66720</b>  | <b>0.203</b>                               | <b>0.083825</b> | <b>0.071</b>                               | <b>0.740</b>        | <b>519.4</b>              | <b>3.5</b>                                    | <b>519.01</b>                                | <b>0.82</b>                                  | <b>518.91</b> | <b>0.35</b> |  |
| <b>z4</b>   | <b>0.197</b> | <b>1.402</b>                                  | <b>99.7</b>  | <b>80</b>                 | <b>0.41</b>    | <b>5193</b>     | <b>0.062</b>                                | <b>0.05771</b>                              | <b>0.096</b>                                | <b>0.66694</b>  | <b>0.150</b>                               | <b>0.083824</b> | <b>0.065</b>                               | <b>0.898</b>        | <b>518.6</b>              | <b>2.1</b>                                    | <b>518.85</b>                                | <b>0.61</b>                                  | <b>518.91</b> | <b>0.32</b> |  |
| z6  | 0.212        | 0.485   | 98.9         | 25                        | 0.45           | 1637            | 0.066                                       | 0.05768                                     | 0.248                                       | 0.66530         | 0.293                                      | 0.083662        | 0.083                                      | 0.650               | 517.4                     | 5.4   | 517.85                                       | 1.19   | 517.94        | 0.41        |  |
| Weighted mean <sup>206</sup> Pb/ <sup>238</sup> U age = 518.99 ± 0.14 (0.20) [0.58] Ma (2 s); MSWD = 0.38 (n = 6) (h) |              |   |              |                           |                |                 |   |   |   |                 |  |                 |  |                     |                           |   |  |  |               |             |  |
| <b>Ti-Am-0.0</b>  |              |   |              |                           |                |                 |   |   |   |                 |  |                 |  |                     |                           |   |  |  |               |             |  |
| <b>z3</b>   | <b>0.184</b> | <b>1.449</b>                                  | <b>99.5</b>  | <b>54</b>                 | <b>0.62</b>    | <b>3502</b>     | <b>0.058</b>                                | <b>0.05774</b>                              | <b>0.113</b>                                | <b>0.66800</b>  | <b>0.165</b>                               | <b>0.083901</b> | <b>0.065</b>                               | <b>0.862</b>        | <b>520.1</b>              | <b>2.5</b>                                    | <b>519.50</b>                                | <b>0.67</b>                                  | <b>519.37</b> | <b>0.33</b> |  |
| <b>z6</b>   | <b>0.235</b> | <b>1.168</b>                                  | <b>99.5</b>  | <b>53</b>                 | <b>0.52</b>    | <b>3395</b>     | <b>0.073</b>                                | <b>0.05777</b>                              | <b>0.123</b>                                | <b>0.66814</b>  | <b>0.173</b>                               | <b>0.083886</b> | <b>0.065</b>                               | <b>0.840</b>        | <b>520.9</b>              | <b>2.7</b>                                    | <b>519.58</b>                                | <b>0.70</b>                                  | <b>519.28</b> | <b>0.33</b> |  |
| <b>z5</b>   | <b>0.228</b> | <b>1.085</b>                                  | <b>99.5</b>  | <b>51</b>                 | <b>0.50</b>    | <b>3292</b>     | <b>0.071</b>                                | <b>0.05789</b>                              | <b>0.152</b>                                | <b>0.66952</b>  | <b>0.218</b>                               | <b>0.083881</b> | <b>0.116</b>                               | <b>0.753</b>        | <b>525.6</b>              | <b>3.3</b>                                    | <b>520.42</b>                                | <b>0.89</b>                                  | <b>519.25</b> | <b>0.58</b> |  |
| <b>z2</b>   | <b>0.257</b> | <b>2.404</b>                                  | <b>99.8</b>  | <b>118</b>                | <b>0.48</b>    | <b>7528</b>     | <b>0.080</b>                                | <b>0.05777</b>                              | <b>0.085</b>                                | <b>0.66813</b>  | <b>0.141</b>                               | <b>0.083876</b> | <b>0.065</b>                               | <b>0.918</b>        | <b>521.1</b>              | <b>1.9</b>                                    | <b>519.57</b>                                | <b>0.57</b>                                  | <b>519.21</b> | <b>0.32</b> |  |
| <b>z7</b>   | <b>0.242</b> | <b>1.826</b>                                  | <b>99.8</b>  | <b>113</b>                | <b>0.38</b>    | <b>7255</b>     | <b>0.076</b>                                | <b>0.05780</b>                              | <b>0.086</b>                                | <b>0.66830</b>  | <b>0.142</b>                               | <b>0.083864</b> | <b>0.066</b>                               | <b>0.921</b>        | <b>522.0</b>              | <b>1.9</b>                                    | <b>519.68</b>                                | <b>0.58</b>                                  | <b>519.15</b> | <b>0.33</b> |  |
| <b>z4</b>   | <b>0.186</b> | <b>2.380</b>                                  | <b>99.8</b>  | <b>144</b>                | <b>0.38</b>    | <b>9375</b>     | <b>0.058</b>                                | <b>0.05775</b>                              | <b>0.077</b>                                | <b>0.66775</b>  | <b>0.135</b>                               | <b>0.083862</b> | <b>0.064</b>                               | <b>0.946</b>        | <b>520.3</b>              | <b>1.7</b>                                    | <b>519.34</b>                                | <b>0.55</b>                                  | <b>519.13</b> | <b>0.32</b> |  |
| z1  | 0.199        | 1.896   | 99.7         | 93                        | 0.47           | 6076            | 0.062                                       | 0.05768                                     | 0.091                                       | 0.66638         | 0.146                                      | 0.083789        | 0.065                                      | 0.908               | 517.7                     | 2.0   | 518.51                                       | 0.59   | 518.70        | 0.33        |  |



|   |              |              |              |            |             |              |              |                |              |                |              |                 |              |              |              |            |               |             |               |             |
|---|--------------|--------------|--------------|------------|-------------|--------------|--------------|----------------|--------------|----------------|--------------|-----------------|--------------|--------------|--------------|------------|---------------|-------------|---------------|-------------|
| Weighted mean <sup>206</sup> Pb/ <sup>238</sup> U age = 519.23 ± 0.14 (0.21) [0.58] Ma (2 s); MSWD = 0.29 (n = 6) (h) |              |              |              |            |             |              |              |                |              |                |              |                 |              |              |              |            |               |             |               |             |
| <b>Ti-I-neg8.5</b>  |              |              |              |            |             |              |              |                |              |                |              |                 |              |              |              |            |               |             |               |             |
| z8  | 0.648        | 0.473        | 99.6         | 74         | 0.17        | 4270         | 0.202        | 0.05789        | 0.133        | 0.67734        | 0.181        | 0.084862        | 0.069        | 0.798        | 525.6        | 2.9        | 525.17        | 0.74        | 525.08        | 0.35        |
| <b>z4</b>   | <b>0.255</b> | <b>0.893</b> | <b>99.6</b>  | <b>79</b>  | <b>0.27</b> | <b>5036</b>  | <b>0.080</b> | <b>0.05781</b> | <b>0.100</b> | <b>0.66977</b> | <b>0.157</b> | <b>0.084024</b> | <b>0.073</b> | <b>0.865</b> | <b>522.7</b> | <b>2.2</b> | <b>520.57</b> | <b>0.64</b> | <b>520.09</b> | <b>0.37</b> |
| <b>z1</b>   | <b>0.288</b> | <b>2.044</b> | <b>99.9</b>  | <b>244</b> | <b>0.20</b> | <b>15440</b> | <b>0.090</b> | <b>0.05774</b> | <b>0.069</b> | <b>0.66842</b> | <b>0.129</b> | <b>0.083958</b> | <b>0.065</b> | <b>0.960</b> | <b>520.0</b> | <b>1.5</b> | <b>519.75</b> | <b>0.52</b> | <b>519.70</b> | <b>0.32</b> |
| Weighted mean <sup>206</sup> Pb/ <sup>238</sup> U age = 519.87 ± 0.24 (0.35) [0.64] Ma (2 s); MSWD = 2.60 (n = 2) (h) |              |              |              |            |             |              |              |                |              |                |              |                 |              |              |              |            |               |             |               |             |
| <b>Tiout-566</b>  |              |              |              |            |             |              |              |                |              |                |              |                 |              |              |              |            |               |             |               |             |
| <b>z5</b>   | <b>0.348</b> | <b>0.501</b> | <b>99.1%</b> | <b>33</b>  | <b>0.36</b> | <b>2100</b>  | <b>0.109</b> | <b>0.05757</b> | <b>0.213</b> | <b>0.66854</b> | <b>0.244</b> | <b>0.084228</b> | <b>0.068</b> | <b>0.565</b> | <b>513.3</b> | <b>4.7</b> | <b>519.82</b> | <b>0.99</b> | <b>521.31</b> | <b>0.34</b> |
| <b>z7</b>   | <b>0.231</b> | <b>1.047</b> | <b>99.5%</b> | <b>57</b>  | <b>0.42</b> | <b>3710</b>  | <b>0.072</b> | <b>0.05792</b> | <b>0.104</b> | <b>0.67240</b> | <b>0.137</b> | <b>0.084195</b> | <b>0.053</b> | <b>0.738</b> | <b>526.8</b> | <b>2.3</b> | <b>522.17</b> | <b>0.56</b> | <b>521.11</b> | <b>0.26</b> |
| <b>z2</b>   | <b>0.299</b> | <b>0.450</b> | <b>98.9%</b> | <b>27</b>  | <b>0.40</b> | <b>1701</b>  | <b>0.093</b> | <b>0.05797</b> | <b>0.220</b> | <b>0.67290</b> | <b>0.254</b> | <b>0.084192</b> | <b>0.069</b> | <b>0.605</b> | <b>528.5</b> | <b>4.8</b> | <b>522.47</b> | <b>1.04</b> | <b>521.09</b> | <b>0.35</b> |
| <b>z4</b>   | <b>0.331</b> | <b>0.576</b> | <b>99.3%</b> | <b>41</b>  | <b>0.34</b> | <b>2577</b>  | <b>0.103</b> | <b>0.05792</b> | <b>0.190</b> | <b>0.67230</b> | <b>0.221</b> | <b>0.084180</b> | <b>0.068</b> | <b>0.578</b> | <b>526.9</b> | <b>4.2</b> | <b>522.11</b> | <b>0.90</b> | <b>521.02</b> | <b>0.34</b> |
| <b>z6</b>   | <b>0.259</b> | <b>0.823</b> | <b>99.0%</b> | <b>27</b>  | <b>0.71</b> | <b>1743</b>  | <b>0.081</b> | <b>0.05792</b> | <b>0.152</b> | <b>0.67223</b> | <b>0.183</b> | <b>0.084178</b> | <b>0.052</b> | <b>0.686</b> | <b>526.7</b> | <b>3.3</b> | <b>522.07</b> | <b>0.75</b> | <b>521.01</b> | <b>0.26</b> |
| <b>z1</b>   | <b>0.326</b> | <b>0.423</b> | <b>98.3%</b> | <b>17</b>  | <b>0.60</b> | <b>1070</b>  | <b>0.102</b> | <b>0.05793</b> | <b>0.296</b> | <b>0.67225</b> | <b>0.333</b> | <b>0.084163</b> | <b>0.074</b> | <b>0.579</b> | <b>527.1</b> | <b>6.5</b> | <b>522.08</b> | <b>1.36</b> | <b>520.92</b> | <b>0.37</b> |
| <b>z3</b>   | <b>0.301</b> | <b>0.305</b> | <b>98.7%</b> | <b>22</b>  | <b>0.33</b> | <b>1389</b>  | <b>0.094</b> | <b>0.05737</b> | <b>0.277</b> | <b>0.66566</b> | <b>0.314</b> | <b>0.084158</b> | <b>0.085</b> | <b>0.538</b> | <b>505.6</b> | <b>6.1</b> | <b>518.07</b> | <b>1.27</b> | <b>520.89</b> | <b>0.43</b> |
| Weighted mean <sup>206</sup> Pb/ <sup>238</sup> U age = 521.06 ± 0.12 (0.28) [0.61] Ma (2 s); MSWD = 0.61 (n = 7) (h) |              |              |              |            |             |              |              |                |              |                |              |                 |              |              |              |            |               |             |               |             |

(a)z1, z2 etc. are labels for zircon fragments annealed and chemically abraded after Mattinson (2005); data formatted in bold are included weighted mean calculation.

(b)Model Th/U ratio calculated from radiogenic <sup>208</sup>Pb/<sup>206</sup>Pb ratio and <sup>207</sup>Pb/<sup>235</sup>U date.

(c)Pb\* and Pbc are radiogenic and common Pb, respectively. Mol % <sup>206</sup>Pb\* is with respect to radiogenic and blank Pb.

(d)Measured ratio corrected for spike and fractionation only. Samples were spiked with the ET535 tracer, with an internal U fractionation correction based on the measured <sup>233</sup>U/<sup>235</sup>U, and an external Pb fractionation correction of 0.16 ± 0.02 (1-sigma) %/amu (atomic mass unit), based on analysis of double Pb ET2535 spiked samples over the same analytical period.

(e)Corrected for fractionation, spike, common Pb and initial disequilibrium in <sup>230</sup>Th/<sup>238</sup>U. Up to 0.5 pg of common Pb is assigned to procedural blank with composition of <sup>206</sup>Pb/<sup>204</sup>Pb = 18.042 ± 0.61%; <sup>207</sup>Pb/<sup>204</sup>Pb = 15.537 ± 0.52%; <sup>208</sup>Pb/<sup>204</sup>Pb = 37.686 ± 0.63% (1-sigma). Excess over blank was assigned to initial common Pb, using the Stacey & Kramers (1975) two-stage Pb isotope evolution model at 520 Ma.

(f)Errors are 2-sigma, propagated using algorithms of Schmitz & Schoene (2007). Corr. coeff. - correlation coefficient.

(g)Calculations based on the decay constants of Jaffey et al. (1971). <sup>206</sup>Pb/<sup>238</sup>U and <sup>207</sup>Pb/<sup>206</sup>Pb ratios and dates corrected for initial disequilibrium in <sup>230</sup>Th/<sup>238</sup>U using Th/U [magma] = 3.

(h)Uncertainties listed as ± analytical (analytical + tracer) [analytical + tracer + decay constant] error; MSWD = mean squared weighted deviation.

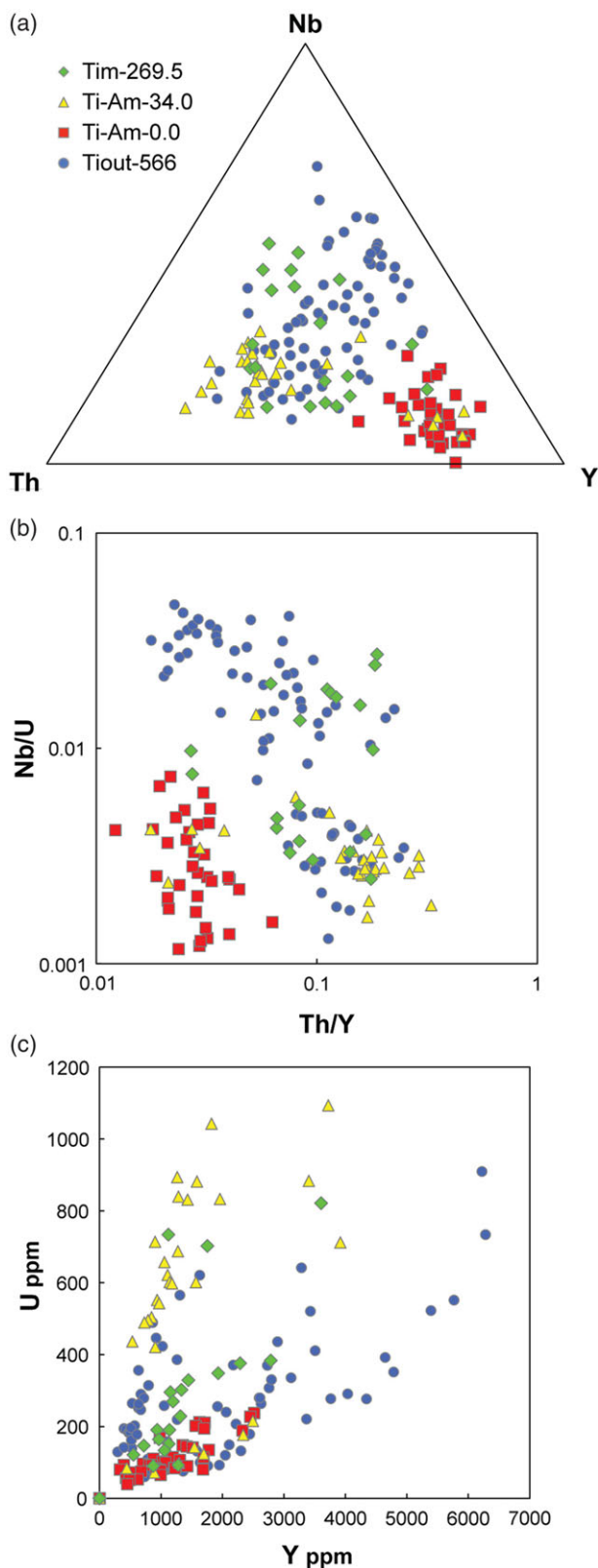


**Fig. 5.** (Colour online) Ternary and bivariate diagrams illustrating variation in zircon geochemistry for four volcanic ash beds of the upper Lie de vin Formation and Amouslek Formation, southern Morocco. Zircon geochemistry was measured by spot LA-ICP-MS analysis.

indicating that any magmatic complexity in the crystal population is minor compared with the analytical variance; the weighted mean date is therefore interpreted as the depositional age of the tuff horizon.

#### 4.b. *Ti-I-neg8.5*

This 1.5-cm-thick, brown-weathering, dolomitic feldspathic sandstone layer is 8.5 m below trilobite horizon T1 (base of *Hupetina antiqua* Zone) and in the uppermost part of the lower member of the Igoudine Formation. The sample has abundant, sub-rounded, white to pink feldspars and lapilli-sized, whitish ash fragments. A sparse sample of small zircon crystals of heterogeneous aspect, rounding, colour and clarity was obtained from this sample; this optical heterogeneity is affirmed in the variation in CL response and internal zoning (online Supplementary Fig. S1). LA-ICP-MS analysis of 18 crystals yielded  $^{206}\text{Pb}/^{238}\text{U}$  dates ranging from the middle Cambrian Period to Palaeoproterozoic Era. Three of the youngest crystals, including two distinctive elongate prismatic zircons with bright CL response, were analysed by CA-ID-TIMS. The latter two crystals gave reproducible  $^{206}\text{Pb}/^{238}\text{U}$  dates with a weighted mean of  $519.87 \pm 0.24$  (0.35) [0.64] Ma (MSWD = 2.60), which is interpreted as a maximum depositional age constraint for this stratigraphic horizon.

#### 4.c. *Ti-XI+1*

This sample comes from a lenticular, 10-cm-thick, reddish-brown weathering dolomitic feldspathic sandstone with large, sub-rounded, white feldspars. The sample horizon is located 1.0 m above trilobite horizon T9 in the upper *Eofallotaspis tioutensis* Zone of the Tiout Member. As for sample Ti-I-neg8.5, this sample yielded sparse, heterogeneous zircon crystals (online Supplementary Fig. S1). LA-ICP-MS analysis of 25 crystals yielded apparent  $^{206}\text{Pb}/^{238}\text{U}$  dates ranging from 1947 to 409 Ma. Given the heterogeneity and discordance of these likely detrital crystals, no further CA-ID-TIMS work was undertaken.

#### 4.d. *Ti-Am-0.0*

Ti-Am-0.0 is a 5–13-cm-thick, yellow-white weathering volcanic tuff with abundant euhedral to subhedral, large white feldspars and occasional grey, rounded, porous lapilli up to 5 mm in diameter. The bed has reworked clasts of lime mudstone and rests unconformably on locally truncated thrombolites at the top of the Tiout Member. This ash is the basal bed of the Amouslek Formation and is assigned here to the transition between the upper *Fallotaspis plana* Zone and lower *Choubertella* Zone.

This tuff sample yielded abundant, sharply faceted, prismatic zircon crystals with a uniform CL response and zoning characterized by brighter interiors and moderately darker margins, often with sector zoning (online Supplementary Fig. S1). LA-ICP-MS spot analyses produced late Ediacaran to dominantly Cambrian apparent ages. Trace-element concentrations and ratios for these zircons are plotted in Figure 5; these compositions define a field distinct from those of the underlying Tiout 566 ash bed in bivariate and ternary spaces. Seven crystals selected for CA-ID-TIMS analysis yielded six concordant and equivalent U–Pb dates, with a weighted mean  $^{206}\text{Pb}/^{238}\text{U}$  date of  $519.23 \pm 0.14$  (0.21) [0.58] Ma (MSWD = 0.29; Fig. 6). A single crystal gave an

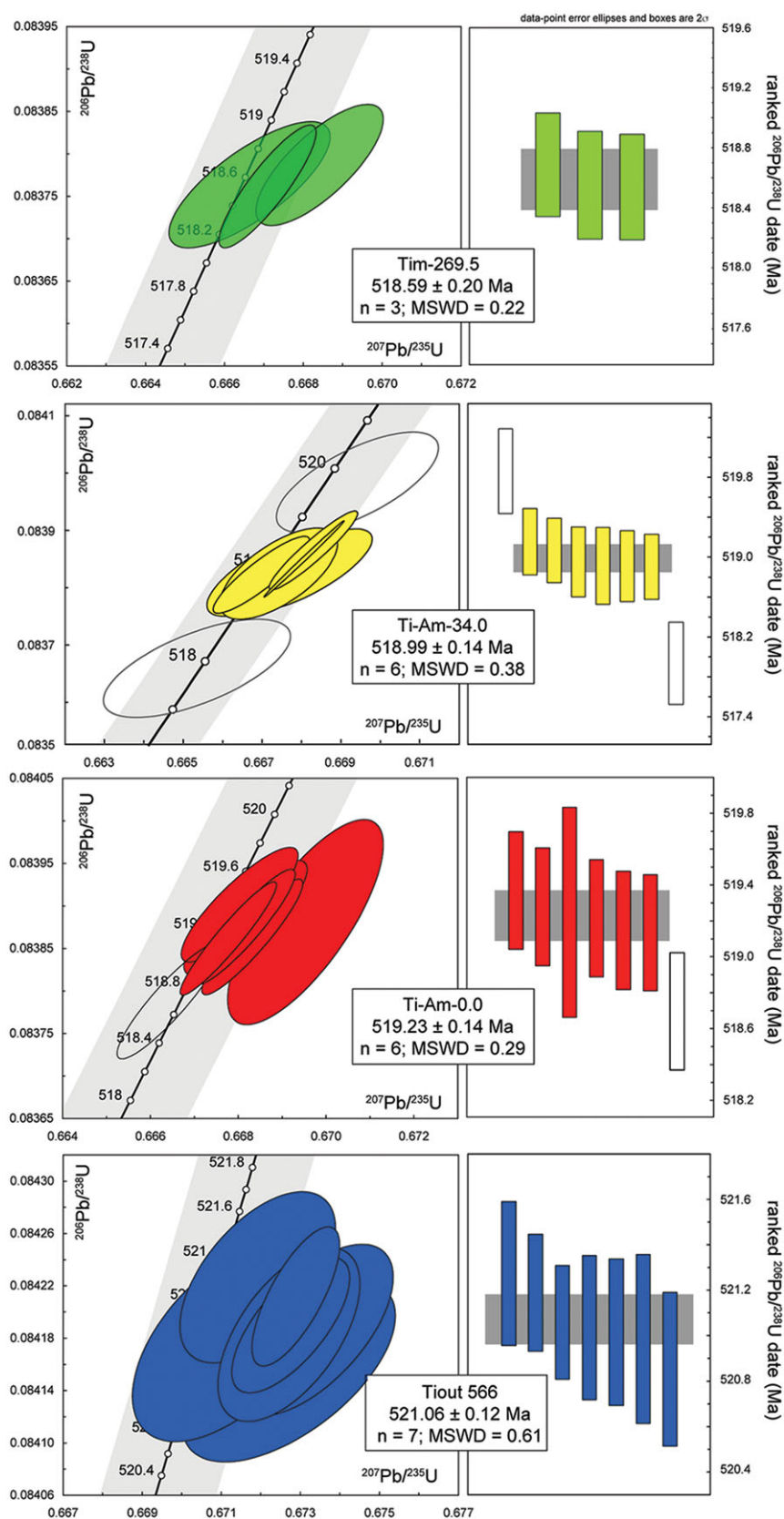


**Fig. 6.** (Colour online) Concordia diagram and ranked  $^{206}\text{Pb}$ – $^{238}\text{U}$  age plots for zircons from volcanic ash beds of the upper Lie de vin Formation and Amouslek Formation, southern Morocco. Zircon ages were measured by CA-ID-TIMS.

anomalously young date attributed to slight residual Pb loss. The weighted mean date of the six texturally, geochemically and geochronologically similar crystals is interpreted to estimate the eruption and deposition of the tuff.

#### 4.e. Ti-Am-34.0

Sample Ti-Am-34.0 is identical in lithology to Ti-Am-0.0. The sample comes from an interval in the lower Amouslek Formation (33.75–34.1 m) not directly bracketed by index fossils. Lithostratigraphic correlation with the neighbouring section at Tazemmourt (e.g. Geyer & Landing, 2006b, p. 60–64, fig. 11) suggests that it belongs to the upper *Choubertella* Zone. The sample horizon lies within a succession of seven thin, current cross-bedded ashes.

This sample yielded abundant, sharply faceted, prismatic zircon crystals from elongate to mostly more equant morphology. CL response revealed a majority of crystals characterized by relatively subdued intensity and superimposed oscillatory zoning, while a handful of crystals were very bright and homogeneous (online Supplementary Fig. S1). LA-ICP-MS spot analyses produced discordant Precambrian results as well as concordant Cambrian apparent ages. Trace-element concentrations and ratios for these zircons are distinct from the underlying Tiout 566 and Ti-Am-0.0 ash beds in bivariate and ternary spaces, particularly in their high actinide concentrations (Fig. 5). Eight crystals selected for CA-ID-TIMS analysis yielded six concordant and equivalent U–Pb dates, with a weighted mean  $^{206}\text{Pb}/^{238}\text{U}$  date of  $518.99 \pm 0.14$  (0.20) [0.58] Ma (MSWD = 0.38; Fig. 6), which is interpreted to estimate the eruption and deposition of the tuff. A single crystal gave a resolvably young date attributed to slight residual Pb loss, unsurprising given the higher U concentrations in this crystal. A second crystal belonging to the minority bright CL intensity subpopulation gave a resolvably older age, consistent with crystal inheritance as the origin of these anomalous grains.

#### 4.f. Tim-269.5

Sample Tim-269.5 from the Timoulaye Izder section is a fairly indurated, calcareous, light-yellowish-grey ash bed with unrounded, sand-sized ash fragments. This ash produced a modest sample of relatively small, faceted zircon crystals, which are admittedly somewhat heterogeneous in CL response. LA-ICP-MS spot analyses on 35 crystals recovered indications of a bimodal crystal population, including an inherited *c.* 2.0 Ga component comprising mostly CL-dark crystals, and a Cambrian component comprising mostly crystals with moderate to bright CL intensity. Eight crystals were selected from the latter group for CA-ID-TIMS analysis. Of these crystals, five of those with the brightest CL response yielded obvious inheritance ages of 522–603 Ma; the remaining three crystals are concordant and equivalent in isotope ratios, with a weighted mean  $^{206}\text{Pb}/^{238}\text{U}$  date of  $518.59 \pm 0.20$  (0.32) [0.63] Ma (MSWD = 0.22; Fig. 6), which is interpreted to estimate the eruption and deposition of the tuff and is a date within the transition between the *Choubertella* and *Daguinaspis* Zones.

#### 4.g. Bayesian age model

We conditioned the modifiedBchron age model for the Tiout section with the four volcanic ash bed depositional ages from

the upper Lie de vin Formation and Amouslek Formation, as well as the maximum depositional age constraint from the volcanic sandstone (sample Ti-I-neg8.5) near the base of the Tiout Member. The position of the ash bed at Timoulaye Idzer was projected into the Tiout section by proportional scaling of the thickness of the Amouslek formation and the appearance of *Daguinaspis* trilobites at each section, with an associated stratigraphic uncertainty. Similarly, the position of the base of the *Choubertella* Zone and top of the *Daguinaspis* Zone at Tiout were projected via proportional scaling from their better-constrained positions in the Timoulaye Idzer section, with secondary control from the nearby Tazemmourt section. Weighted mean ages and their normally distributed standard errors were used for the ash bed depositional ages. We constructed a probability density function for the detrital maximum depositional age by applying a uniform probability between the weighted mean age of the youngest detrital zircons from Ti-I-neg8.5 and that of the next overlying depositional age (ash Ti-Am-0.0; Fig. 7). This complex probability density function was approximated by a stack of uniform probability functions grouped at the sample horizon depth.

Two age models are illustrated in Figure 7; the median (most likely) paths of each model are indicated by solid lines, with the 95% highest density interval shown as a shaded or dashed envelope. A model constructed solely with the volcanic ash beds is illustrated with the red solid and dashed lines. For comparison, the age model with the detrital zircon maximum depositional age constraint is shown by the black median line and surrounding grey envelope encompassing the 95% highest density interval. Although the addition of the detrital zircon constraint makes a minor difference in the median age model, its inclusion significantly shrinks the uncertainty envelope in its vicinity. The refinement to the older side of the age model is a simple consequence of superpositional constraints based on the maximum depositional age constraint at the sandstone horizon. The refinement on the younger side of the age model is related to the interaction of the sedimentation model prior and the full set of conditioning ages, namely the tendency of the prior to minimize changes in accumulation rate, thus lowering the probability of paths that seek the younger end of the maximum depositional age likelihood. This effect is further illustrated in the inset of Figure 7, which superposes the starting likelihood with the posterior probability for the age of the Ti-I-neg8.5 horizon.

Table 2 documents the results of the age model for specific horizons of interest in the Tiout section. Stratigraphic levels are reported with respect to a base at the position of the Tiout 566 volcanic ash bed in the upper Lie de vin Formation. The first occurrence of trilobite fragments in the upper portion of the informal lower member of the Igoudine Formation is dated as  $519.95 + 0.43/- 0.40$  Ma, while the first identifiable trilobite occurrence in the lower Tiout Member defines the base of the *Hupetina antiqua* Zone, dated as  $519.78 + 0.26/- 0.37$  Ma. The *Hupetina antiqua* through *Daguinaspis* zonal succession that defines the Issendalenian Stage is quantitatively calibrated with this age model to range up to  $518.43 + 0.25/- 0.69$  Ma. Individual zones span approximately 0.2 Ma, with the exception of the longer *Fallotaspis plana* Zone (0.7 Ma). The first appearance of archaeocyaths 15 m above the base of the Tiout Member of the Igoudine Formation is dated at  $519.71 + 0.26/- 0.35$  Ma.

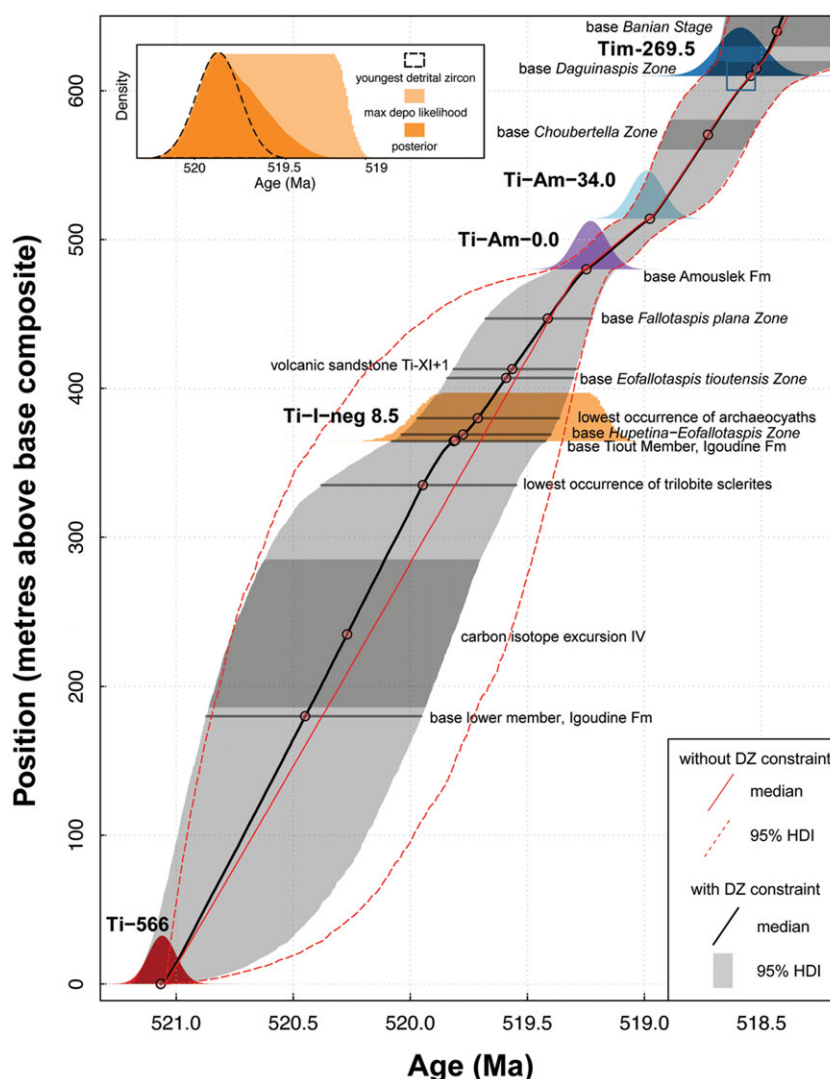


**Fig. 7.** (Colour online) Bayesian age model for the Tiout section, southern Morocco, constructed using the modifiedBchron R package of Trayler *et al.* (2019). Inset illustrates the conditioned posterior probability relative to the starting likelihood function of the detrital zircon maximum depositional age for the volcanic sandstone horizon Ti-I-neg8.5. Model suggests no significant duration of sub-Amouslek sequence boundary. DZ – detrital zircon.

## 5. Discussion

### 5.a. Interregional biostratigraphic correlation of the Tiout Member

The most certain, albeit tentative, correlation of the Tiout Member faunas is with the similar West Gondwanan assemblages of the Ovetian Stage in southern Spain (i.e. the Ossa-Morena zone). Here, the joint lowest occurrence of archaeocyaths (Zone I of the composite archaeocyath zonation of Perejón, 1986, 1994) and trilobites (bigotinids) has been used to define the base of the Spanish Ovetian Stage (Liñán *et al.* 1993). As at Tiout, the lowest occurrence of these macrofossils lies at a facies change into more carbonate-rich, shallow, higher energy shelf facies in Spain (Liñán *et al.* 1993). Perejón's (1986) succession of 11 lower Cambrian archaeocyath zones is more finely divided than the Moroccan archaeocyath succession.

However, the Spanish archaeocyath zonation is a composite succession developed from localities across Spain. The zonation shows little vertical change in taxonomic composition, with most taxa appearing low in the 'succession' and persisting to the top.

Geyer & Landing (2004, p. 183) suggested that key differences through the Spanish zonation reflect collecting bias with genera 'appearing' and 'disappearing' with changes in diversity of the successive assemblages. The lower six or so Spanish archaeocyath zones of the Ovetian have been broadly correlated with the West Gondwanan Issendalenian Stage as developed in Morocco (Debrenne & Debrenne, 1995; Zhuravlev, 1995; Geyer & Landing, 2004). Unfortunately, the relatively low-diversity Ovetian trilobite faunas feature shallow-water genera that do not allow a precise correlation into the Issendalenian of Morocco (Geyer & Landing, 2004). It is possible that the abrupt appearances of archaeocyaths and trilobites in Iberia and southern Morocco reflect deepening by a combination of roughly coeval epirogenic/eustatic changes on the Moroccan-Iberian margin of the West Gondwanan shelf, which would be a development similar to the linked lithofacies and faunal changes in the lower-middle Cambrian boundary interval of southern Morocco and northern Iberia (Landing *et al.* 2006).

One of the anchors claimed to supply a confident correlation between the Spanish Ovetian horizons with the Moroccan Anti-Atlas and a claimed very early age of the lower Ovetian is

**Table 2.** Bayesian age model results for the Tiout section, southern Morocco

| Composite position (metres above base) | Event                                     | Likelihood age (Ma, $\pm$ 95% confidence interval) | Posterior age (Ma, $\pm$ 95% highest density interval) | Formation or member |
|--|---|--|--|---------------------|
| 640 $\pm$ 10                           | Base Banian Stage                         |  | 518.43 + 0.25/– 0.69                                   | Amouslek            |
| 615 $\pm$ 10                           | Base <i>Daginaspis</i> Zone               |  | 518.52 + 0.22/– 0.41                                   | Amouslek            |
| 610 $\pm$ 10                           | Ash Tim-269.5 (correlated)                | 518.59 $\pm$ 0.20                                  | 518.55 + 0.26/– 0.44                                   | Amouslek            |
| 570 $\pm$ 10                           | Base <i>Choubertella</i> Zone             |  | 518.73 + 0.21/– 0.22                                   | Amouslek            |
| 514 $\pm$ 0.1                          | Ash Ti-Am-34.0                            | 518.99 $\pm$ 0.14                                  | 518.98 + 0.12/– 0.13                                   | Amouslek            |
| 480 $\pm$ 0.1                          | Ash Ti-Am-0.0; base Amouslek Formation    | 519.23 $\pm$ 0.14                                  | 519.25 + 0.13/– 0.13                                   | Amouslek            |
| 447 $\pm$ 1                            | Base <i>Fallotaspis plana</i> Zone        |  | 519.41 + 0.27/– 0.19                                   | Igoudine/Tiout      |
| 413 $\pm$ 0.1                          | Volcanic sandstone Ti-XI + 1              |  | 519.56 + 0.25/– 0.27                                   | Igoudine/Tiout      |
| 407 $\pm$ 1                            | Base <i>Eofallotaspis tioutensis</i> Zone |  | 519.59 + 0.25/– 0.29                                   | Igoudine/Tiout      |
| 380 $\pm$ 0.1                          | Lowest occurrence of archaeocyaths        |  | 519.71 + 0.26/– 0.35                                   | Igoudine/Tiout      |
| 369 $\pm$ 0.1                          | Base <i>Hupetina antiqua</i> Zone         |  | 519.78 + 0.26/– 0.37                                   | Igoudine/Tiout      |
| 365 $\pm$ 0.1                          | Base Tiout Member                         |  | 519.81 + 0.26/– 0.39                                   | Igoudine/Tiout      |
| 364.5 $\pm$ 0.1                        | Volcanic sandstone Ti-I-neg8.5            | $\leq$ 519.89 $\pm$ 0.24                           | 519.82 + 0.26/– 0.39                                   | Igoudine/lower      |
| 335 $\pm$ 1                            | Lowest occurrence of trilobite debris     |  | 519.95 + 0.43/– 0.40                                   | Igoudine/lower      |
| 235 $\pm$ 50                           | Carbon isotope excursion IV               |  | 520.27 + 0.59/– 0.57                                   | Igoudine/lower      |
| 180 $\pm$ 1                            | Base informal lower member                |  | 520.45 + 0.42/– 0.50                                   | Igoudine/lower      |
| 0 $\pm$ 0.1                            | Ash Tiout 566                             | 521.06 $\pm$ 0.12                                  | 521.07 + 0.12/– 0.12                                   | Lie de vin/upper    |

the occurrence of *Lemdadella* in both regions (i.e. Liñán & Sdzuy, 1978). The latter authors assigned *Lemdadella tioutensis* to the *F. tazemmourtensis* Zone and used the species for a correlation with the *Lemdadella linaresae*-bearing strata in the Pedroche Formation of the Córdoba area, southern Spain. Another taxon assigned to *Lemdadella* (i.e. *L. perejoni*) was later described from strata overlying those with *L. linaresae* (Liñán *et al.* 2008a).

*Lemdadella* may be very geographically widespread in Gondwana, and another species, *L. antarctica*, is recorded from the Shackleton Limestone in the central Transantarctic Mountains (Palmer & Rowell, 1995). However, careful restudy is needed to confirm this generic assignment.

Arguments for using *Lemdadella tioutensis*, or *Lemdadella* in general, for relatively precise correlation of the Iberian archaeocyath zone III into the *F. tazemmourtensis* (now *F. plana*) Zone (e.g. Liñán & Sdzuy, 1978; Liñán *et al.* 2008b) remain unconvincing as these forms are lithofacies-associated taxa and include named species that are very restricted palaeogeographically. In addition, the locally abundant species *L. linaresae*, as well as *L. perejoni*, from the Iberian Ossa–Morena zone show distinct differences from Moroccan *L. tioutensis* and probably represent a different genus (G. Geyer, unpublished data). Later collection of bigotinid trilobites below the *Lemdadella linaresae* Zone in Iberia and the resultant suggestion of three more trilobite zones below it are based on monospecific occurrences of trilobites in Iberian archaeocyath Zones I–III. A recent description of the monospecific fauna with *Lunolenus antiquus* (Sdzuy, 1961) in the La Herrería Formation at Barrios de Luna in the Cantabrian Mountains and its tentative correlation with the lowest Ovetrian archaeocyath zones (Liñán *et al.* 2008b) is based on arguments that may be questioned.

Intercontinental correlations of the lowest faunas of the West Gondwanan Issendalenian Stage have emphasized

archaeocyath-based correlations that have led to contradictory correlation into the lower Cambrian strata of SE Siberia. By one proposal (e.g. Debrenne & Debrenne, 1995; Zhuravlev, 1995), the Moroccan lower archaeocyath interval (*Erismacoscinus fasciola* – *Retecoscinus minutus* Zone) and the entire Tiout Member and lower Issendalenian Stage are equated with the lowest archaeocyaths (*Retecoscinus zegebarti* Zone) that define the base of the Siberian Atdabanian Stage. Alternatively, the *E. fasciola* – *R. minutus* Zone has been claimed to correlate with the upper Atdabanian Stage (Rožanov & Debrenne, 1974; Magaritz *et al.* 1991).

Confusingly, the overlying Moroccan *Erismacoscinus maroccanus* Zone, as well as the upper Issendalenian Stage, Amouslek Formation and traditional *Fallotaspis tazemmourtensis* – *Choubertella* – *Daginaspis* zones have also been generally equated with the middle–upper Atdabanian Stage (Debrenne & Debrenne, 1995; Zhuravlev, 1995). A reason for this may be seen in the relatively small changes in the composition of the assemblages that preclude definition of biostratigraphically distinct zones. The problem with correlation of the lowest Moroccan archaeocyaths with those that define the base of the Atdabanian Stage is that the lowest appearances of Siberian *Retecoscinus zegebarti* Zone archaeocyaths and the oldest Atdabanian trilobites (*Profallotaspis jakutensis* Zone) are similar to the Moroccan and Spanish lowest trilobites and archaeocyaths in that all these taxa appear at a distinct lithofacies change.

As discussed by Landing *et al.* (2013), 35 m of reddish mudstones and carbonates on the Lena River are assigned in many reports (e.g. Varlamov *et al.* 2008) to the upper Tommotian Stage and *Dokidocyathus lenaicus* Zone, even though no archaeocyaths or other macrofossils are present. This interval is abruptly succeeded by strata with thin planar thrombolites with the reappearance of archaeocyaths (*R. zegebarti* Zone) and lowest

known trilobites (*Profallotaspis jakutensis* Zone) 2.6 m higher (e.g. Varlamov *et al.* 2008, figs 30, 34). The *Retecoscinus* zones of southern Morocco and SE Siberia can therefore only be considered to be similar in taxonomic (generic) composition, but a confident geochronologic correlation is not possible as the earliest record of archaeocyaths and trilobites of both regions corresponds to the lithofacies changes in the Moroccan and Siberian successions, and the prior record of both biotic groups is absent.

### 5.b. Carbon isotope-based global correlation of upper lower Cambrian System

A resolution of the interregional correlation of the oldest Moroccan archaeocyaths and identifiable trilobites seems possible with  $\delta^{13}\text{C}$  chemostratigraphy. Early reconnaissance work at Tiout by Tucker (1986) and Kirschvink *et al.* (1991) demonstrated a positive  $\delta^{13}\text{C}$  excursion that peaks slightly below the middle of the traditional 'Calcaire supérieur' (middle of the lower member of the Igoudine Formation) and c. 130 m below the base of the Tiout Member (Kirschvink *et al.* 1991, fig. 3). This positive shift in the lower Igoudine Formation seems to be present in the more closely spaced samples at the nearby Oued Sdas section (Fig. 1) as indicated by increasing  $\delta^{13}\text{C}$  values to the top of the sampled section (Malooof *et al.* 2005, fig. 2). Correlation of the  $\delta^{13}\text{C}$  chemostratigraphy between the Tiout and Oued Sdas sections is confirmed in this study by ash beds in the two sections dated to the same age within the margin of error (Tiout 566 at  $521.06 \pm 0.12$  Ma and M236 at  $520.93 \pm 0.14$  Ma in the Lie de vin Formation). The calculated age of the strong, positive  $\delta^{13}\text{C}$  excursion higher in the Tiout succession in the lower Igoudine Formation is  $520.27 + 0.59/- 0.57$  Ma (Fig. 7).

The distinct  $\delta^{13}\text{C}$  positive excursion at Tiout and Oued Sdas has been correlated with the cycle IV excursion in the lower but not lowermost Atdabanian Stage (i.e. within the *Repinaella* Zone) in Siberia (Brasier & Cowie, 1989; Kirschvink *et al.* 1991; Malooof *et al.* 2005, 2010; Landing *et al.* 2013). This correlation, along with equation of the strong negative  $\delta^{13}\text{C}$  excursion in the upper Adoudou Formation with the lowest Tommotian Stage of Siberia (Brasier *et al.* 1991; Magaritz *et al.* 1991; Malooof *et al.* 2005, 2010), would mean that the oldest archaeocyaths and identifiable trilobites in the Tiout Member are younger than the Siberian lower Atdabanian IV carbon excursion. In that case, the two '*Retecoscinus* zones' in Morocco and Siberia are only similar in generic composition but cannot be considered to be coeval, while the *Profallotaspis jakutensis* Zone would be older than the *Hupetina antiqua* Zone.

### 5.c. Appearance of the oldest trilobites

As noted above (Section 2.e), the oldest trilobites and archaeocyaths have abrupt lowest occurrences in the lower Cambrian strata of southern Morocco at lithofacies changes with appearance of higher-energy, less-restricted marine conditions. The known lowest occurrence of identifiable trilobites such as *Hupetina*, *Bigotina* and *Eofallotaspis* may therefore reflect a preservational artefact and not an evolutionary event. More generally, Landing *et al.* (2013, also Geyer & Landing, 2018) argued that the lowest occurrence of early Cambrian trilobites should not be equated with a correlatable evolutionary first appearance datum (FAD) and used to define the base of a global chronostratigraphic Series 2 of the Cambrian (*vide* Peng & Babcock, 2005, 2011; i.e. their 'FAD of trilobites'). Indeed, the lowest local occurrences of the earliest

trilobites overlie unconformities (sometimes cryptic) or may be controlled by the development of favourable habitats/lithofacies for colonization (e.g. southern Morocco, southern Spain, SE Siberian Platform), preservational windows or thoroughness of collecting (Landing *et al.* 2013). In addition, unidentifiable trilobite fragments occur in the lower part of the underlying lower member of the Igoudine Member, which means the simple presence of trilobite fossils may not be a biostratigraphic aid. The biostratigraphic utility of trilobites in sub-Tiout Member strata is therefore limited by preservational artefacts.

Fallotaspids and bigotinids are elements of early trilobite assemblages, but their species are provincial; the mere presence of one of their genera (as '*Fallotaspis*' in the White-Inyo Mountains, SW Laurentia) does not provide a basis for a highly precise correlation. Indeed, *Fallotaspis* has a long stratigraphic range in Morocco where it appears as high as the Issafen Formation (Geyer, 1996; Fig. 2). There has been a desire to apply the early fallotaspid-bearing zonal nomenclature of Morocco to sections worldwide, which led to erroneous identification of archaeaspids as fallotaspids (e.g. Nelson & Hupé, 1964; Khomentovsky & Repina, 1965; Nelson, 1978; Lieberman, 2001). An unfortunate example of this inappropriate use of the Moroccan trilobite zonation in successions where it should not be applied is Rushton *et al.*'s (2011) recognition of the *Eofallotaspis* Zone and a so-called '*Fallotaspis* Zone' as the oldest trilobite zones in Avalonian Britain, even 'though no trilobites definitive of these [endemic] zones are reliably known in British rocks' (Rushton *et al.* 2011, p. 6).

Our new age model provides a high-resolution calibration of the trilobite zones of the Issendalenian Stage. As noted above (sections 2.e, 2.g), the lowest *Fallotaspis plana* (horizon T14) is used to assign the upper range of *Eofallotaspis tioutensis* to the *F. plana* Zone. Volcanic ashes at and above the base of the Amousek with ages of  $519.23 \pm 0.14$  Ma and  $518.99 \pm 0.14$  Ma lie within this *F. plana* Zone and approximate the marine transgression across the Tiout–Amousek hiatus. A volcanic ash dated at  $518.59 \pm 0.20$  Ma just below the *Daguinaspis* Zone at Timoulaye Izder can be confidently correlated to the Tiout section, and thus constrains the timing and duration of the *Choubertella* to *Daguinaspis* Zones to between 518.73 and 518.43 Ma.

This age model assists in global correlation of the highly provincial early Cambrian trilobite faunas. These *Choubertella* to *Daguinaspis* Zone ages are significantly older than the  $517.22 \pm 0.31$  Ma zircon date on a thin ash on the inner platform of Avalon (Landing, 1996) from the lower *Callavia* Zone at Nuneaton, Warwickshire (Williams *et al.* 2013). The Warwickshire *Callavia* Zone date is arithmetically identical to a legacy date of  $517 \pm 1.5$  Ma from the *Antatlasia guttapluyviae* Zone in the Lemdad Formation in the High Atlas (Landing *et al.* 1998; Fig. 2). The perspective here is that *Callavia* had a surprisingly long range in Avalonia from  $517.22 \pm 0.31$  Ma (Williams *et al.* 2013) up to a date of  $514.45 \pm 0.36$  Ma on the Green *Callavia* Sandstone at Comley, Shropshire (Harvey *et al.* 2011).

The unidentified trilobite remains in the basal Caerfai Bay Formation at Caerfai Bay, South Wales (Harkless & Hicks, 1871; Landing *et al.* 2013) have an age of c.  $519 \pm 1$  Ma (Landing *et al.* 1998, 2013). This is comparable to a  $519.30 \pm 0.23$  Ma zircon age from a fault-isolated block of the lowest Caerfai Bay at nearby Cwm Bach (Harvey *et al.* 2011). These c. 519 Ma ages in South Wales are on trilobite remains that may be the oldest in Avalonia. The ages correspond closely to the  $519.95 + 0.45/- 0.39$  Ma age for the oldest sclerites in Morocco, and the

520.28 + 0.51/– 0.44 Ma carbon isotope excursion peak in the lower Igoudine Formation (Fig. 7) that is equated with the peak of the IV carbon isotope excursion in the lower, but not lowermost, trilobite-bearing strata of Siberia (Landing *et al.* 2013; Landing & Kouchinsky, 2016). If the IV excursion peak at Zhurinsky Mys on the Lena River was used as the base of the upper lower Cambrian global Series 2/Lenaldanian Series, as proposed by Landing *et al.* (2013), then the lithofacies-change-associated oldest trilobites in Siberia (*Profallotaspis jakutensis* Zone) would likely only be somewhat older, perhaps *c.* 520 Ma. This definition of the base of Series 2/Lenaldanian Series would allow interregional correlation of the IV excursion of Siberia, into South China (ZHUCE excursion) and, on the basis of this strong carbon excursion, into Avalonia and West Gondwana (lower Igoudine Formation).

Interregional comparison of the oldest identifiable trilobites (based on mineralized sclerites) through radioisotopic geochronology and carbon isotope stratigraphy serves to emphasize that quite distinct taxa comprise the oldest trilobite assemblages on Cambrian palaeocontinents. This means that an unrecorded interval of trilobite origination and diversification preceded the local appearance of the ‘oldest’ mineralized trilobites, with local assemblages comprising *de facto* trilobite faunal provinces (e.g. Fortey *et al.* 1996; Landing *et al.* 2013). Taxonomic differences between the lowest-occurring forms include archaeaspidids and bigotinids on the Siberian Platform and western Laurentia, fallotaspids *s.s.* and bigotinids in West Gondwana (Morocco and Iberia), seemingly significantly younger olenelloids representing endemic genera in southern Baltica and Avalonia, and redlichoids in East Gondwana (South China and Australia).

Very different dates have been proposed for the origin of trilobites as a crown group of euarthropods based on palaeobiogeographical analyses of differences between the oldest local trilobite assemblages. A Cryogenian origin of *c.* 750 Ma was proposed by Fortey *et al.* (1996), while Meert & Lieberman (2004, 2008; also Álvaro *et al.* 2013) suggested an early–late, but not latest, Ediacaran age bracket of *c.* 600–550 Ma. These dates are far older and cannot be reconciled with the body or trace fossil record of trilobites. The oldest arthropod-produced, trace fossils include *Rusophycus* and *Cruziana* in the Avalonian *Rusophycus avalonensis* Ichnofossil Zone and in coeval intervals globally (e.g. review and references in Geyer & Landing, 2017). The upper *Rusophycus avalonensis* Zone has a *c.* 530 Ma U–Pb legacy age determined in Avalonian New Brunswick (Landing *et al.* 1998). Ichnofossils from the *R. avalonensis* Zone precede the oldest known mineralized trilobite remains at *c.* 520 Ma as suggested here on the basis of interregional correlation of the Siberian IV carbon isotope excursion. There is an obvious morphologic similarity of traces from the *R. avalonensis* Zone and coeval intervals to later, likely trilobite-produced, rusophyciform and cruzianaform traces in marine Phanerozoic rocks. This similarity suggests their formation by arthropods that, but for their apparent skeletal nonmineralization, would be trilobites. If so, then the possible 530 Ma or somewhat earlier initial appearance and diversification of trilobites would fall in the later part of the Cambrian Evolutionary Radiation, and not the Ediacaran Evolutionary Radiation (i.e. Landing *et al.* 2018).

#### 5.d. Trilobites and lower Cambrian chronostratigraphy

As discussed above, a ‘FAD of trilobites’ should not be considered as a biostratigraphic criterion to define the base of a global upper lower Cambrian Series 2 (e.g. Peng & Babcock, 2005, 2011), as all

known trilobite first occurrences in the lower Cambrian strata appear above stratigraphic discontinuities defined by unconformities or lithofacies changes. This problem led Landing *et al.* (2013) to propose that the base of Cambrian Series 2, or their proposed Lenaldanian Series, should be defined at the Zhurinsky Mys section on the Lena River in Siberia. The proposed level is somewhat above the lowest local trilobite occurrence (*Profallotaspis jakutensis* Zone) and at the peak of the IV carbon isotope excursion within the *Repinaella* Zone. This would allow interregional correlation of the base of a Series 2/Lenaldanian Series by the IV excursion of Siberia, into South China (ZHUCE excursion) and, on the basis of this strong carbon excursion, into Avalonia and West Gondwana (lower Igoudine Formation). The calculated age of the peak of this excursion in the lower Igoudine Formation is *c.* 520.27 + 0.59/– 0.57 Ma, and this age would apply to the Siberian IV excursion (Malooof *et al.* 2010). In turn, this *c.* 520.3 Ma date would only be slightly younger than that of the oldest mineralized trilobites of the *Profallotaspis jakutensis* Zone that appear *c.* 22 m lower than the IV peak and 2.6 m above a lithofacies break in Siberia (Varlamov *et al.* 2008). In lieu of a Siberian ash date, a *c.* 521 Ma date might be estimated for the oldest Siberian trilobites.

Landing *et al.* (2013) discussed how this proposed definition for the informal Series 2 base would put the oldest known mineralized trilobite remains into the Terreneuvian Series. However, as discussed above, the lowest records of mineralized trilobites lie globally at a stratigraphic discontinuity and do not preserve the early origin and diversification of the group. Definition of a global stratigraphic section and point (GSSP) for the base of Cambrian Series 2 based on a taxon purportedly corresponding to the ‘FAD of trilobites’ means that subsequent recovery of this taxon or another older than the GSSP, which is likely given the undefined confidence interval of fossil taxa (e.g. Marshall, 1990), would demonstrate the limitations of the GSSP. Indeed, the presence of *Rusophycus* and *Cruziana* traces earlier than *c.* 530 Ma that suggests an origin of nonmineralized trilobites during early Terreneuvian time further means that the recovery of mineralized remains is possible in the *c.* 530–520 Ma interval.

#### 5.e. Palaeogeographic consequences of new U–Pb dates

The revised and new U–Pb zircon dates from the Moroccan lower Cambrian strata provide additional information pertinent to reconstructing the palaeogeography of Avalonia and West Gondwana. The most common palaeogeographic reconstruction shows Avalonia very close to or coterminous with the tropical NW African (Moroccan) margin of West Gondwana through the Cambrian Period (e.g. Álvaro *et al.* 2013, fig. 19.1; Murphy *et al.* 2018, fig. 5B). Alternatively, Avalonia was an insular microcontinent separate from Gondwana (with early Cambrian fallotaspidid *s.s.*- and archaeocyath-bearing faunas in a tropical carbonate platform succession) by the end of the Ediacaran Period (e.g. Landing, 1996, 2005; Keppie & Keppie, 2014). Coeval successions in Avalonia, by contrast, have endemic Lower Cambrian faunas in a cool-water shale-platform sequence (with olenelloids, but without archaeocyaths) (Landing, 1996, 2005; Landing & Westrop, 2004; Landing *et al.* 2013, 2017).

The 519–517 Ma U–Pb zircon dates are useful to emphasize conclusions that coeval successions in Avalonia and Moroccan West Gondwana are lithologically and biotically distinctive (see also Landing *et al.* 2013). The two regions cannot be placed in a



palaeogeographic reconstruction in which the two areas are relatively adjacent and only separated by several hundred kilometres) (e.g. Álvaro *et al.* 2013; Murphy *et al.* 2018), and lie in a comparable palaeolatitude (and climatic) setting, but do not have common faunas or biotas through the early Cambrian Period. Álvaro *et al.* (2013, p. 282, fig. 19.1) stated that Avalonia was too far south to have tropical archaeocyaths like Morocco, but showed an 'adjacent' Morocco and Avalonia in their reconstruction at a 'non-tropical' 60° S. They also seem to deny existence of a regional carbonate platform in early Cambrian Morocco (*contra* Geyer & Landing, 1995, 2006a, b) by noting a local carbonate-shale interval in a small transtensional basin in the western Atlas. They also noted that 'fenestral fabrics' in biological build-ups show a tropical location of Avalonia. However, it must be emphasized that fenestral fabrics are not documented in Avalonian Cambrian successions (e.g. Monninger, 1979). Furthermore, the purported palaeolatitudinal significance of fenestrae claimed by Álvaro *et al.* (2013) in microbial build-ups is incorrect, as fenestrae occur even in lacustrine build-ups in modern, high-temperate New York (e.g. Eggleston & Dean, 1976). A simple picture of coeval mudstone-dominated and carbonate platform successions in Avalonia and Morocco hopefully emphasizes that Avalonia and West Gondwana were not adjacent during the early Cambrian Period (Landing *et al.* 2013, fig. 3).

The new and revised U–Pb dates and Bayesian model for lower Cambrian Morocco also help reconstruct the region's palaeogeographic setting. One implication of the dates is the very rapid early Cambrian subsidence of the Souss Basin. Sample Tiout 566 from the upper Lie de vin Formation and sample Ti-Am-0.0 from an ash at the sequence boundary defined by the base of the Amouslek Formation bracket a carbonate-dominated, 600-m-thick platform succession. The rate of accumulation of compacted carbonate rock (c. 220 m Ma<sup>-1</sup>) shown by the Tiout section is among the highest for carbonate platforms through the Phanerozoic Eon (e.g. Bosscher & Schlager, 1993). This indicates that carbonate sediment aggradation kept up with rapid, likely transtensional rift subsidence (Landing *et al.* 2006) to maintain shallow-marine facies.

A likely change of epeirogenic subsidence and sea-level change rates may have led to the transition to less restricted marine-shelf conditions and the appearance of the oldest archaeocyaths and identifiable trilobite assemblages at about the base of the Tiout Member. Changes in either rates of subsidence or sea-level rise or both led to formation of the sequence boundary at the top of the carbonate platform (top of Tiout Member) and seemingly the end of the carbonate platform and its replacement by the mixed siliciclastic-carbonate shelf of the Amouslek Formation. An alternative explanation of this carbonate-mixed-siliciclastic-carbonate shelf transition may be the onset of a southwards movement of the West Gondwanan margin into cooler latitudes during the late early Cambrian Period (Landing & Westrop, 2004; Landing *et al.* 2013).

## 6. Conclusions

New precise U–Pb zircon dates from the Tiout and Timoulaye Izder sections in southern Morocco allow a number of conclusions about the early history of trilobites and archaeocyaths, as well as early Cambrian palaeogeography. Bayesian age modelling constrains the age of the peak of a strong positive carbon isotope

excursion in the lower member of the Igoudine Formation to 520.27 + 0.59/– 0.57 Ma. This date on the lower Igoudine Formation excursion is very important as the Moroccan excursion is correlated with the IV excursion in the lower Atdabanian Stage (*Repinaella* Zone).

Our age model (Fig. 7) shows that the lowest occurrence of trilobite fragments in the lower member of the Igoudine Formation can be dated as 519.95 + 0.43/– 0.40 Ma. This is younger than an estimated c. 521 Ma age of the oldest Siberian trilobites, while the first identifiable trilobite occurrence defining the base of the *Hupetina antiqua* Zone is even younger at 519.78 + 0.26/– 0.37 Ma.

This report demonstrates not only that the lowest occurrence of identifiable West Gondwanan (Moroccan) trilobites lies at a stratigraphic discontinuity (i.e. establishment of less restricted marine facies), but also shows that the global diachrony of the oldest trilobites argued by Landing *et al.* (2013) can now be numerically calculated; the lowest fragmentary Moroccan fauna is at least c. 0.5 Ma younger than the estimated age of the lowest Siberian assemblage. This diachrony also extends to other clades, as the estimated maximum age on the oldest Tommotian Stage archaeocyaths in Siberia is c. 525.5 Ma (Malooof *et al.* 2005, 2010), while new U–Pb dates demonstrate a much younger appearance of the lowest archaeocyaths in the Tiout Member at 519.71 + 0.26/– 0.35 Ma.

After the appearance of mineralized trilobites at an estimated c. 521 Ma, quite rapid changes in traditional (mineralized) trilobites took place. U–Pb dates from southern Morocco quantify those rapid changes through time of the oldest trilobite faunas. The *Hupetina antiqua* – *Eofallotaspis tioutensis* – *Choubertella* – *Daguinaspis* zones succeeded each other in the relatively brief time interval of < 1.5 Ma during c. 519.78 to 518.43 Ma (Fig. 7), with a distinct change of faunal composition.

U–Pb dates from the upper Lie de vin Formation (sample Tiout 566, c. 521.06 Ma) to the lower Amouslek Formation (sample Ti-Am-34, c. 518.99 Ma) demonstrate that c. 634 m of rock was deposited in c. 3 Ma, yielding an average rate of accumulation of compacted rock of slightly more than 220 m Ma<sup>-1</sup>. Finally, c. 519–517 Ma dates from Morocco and Avalonia further emphasize the distinctiveness of coeval biotas and lithofacies of the West Gondwanan (Moroccan) carbonate platform and Avalonian siliciclastic shelf. Although commonly illustrated as adjacent or even coterminous, Avalonia existed as an insular continent by the late Ediacaran Period and was latitudinally separate from the West Gondwanan margin through the early Cambrian Period as shown by the distinctive lithofacies and biotas of the two regions.

**Acknowledgments.** Funding for the analytical infrastructure of the Boise State Isotope Geology Laboratory was provided by the NSF Major Research Instrumentation grants EAR-0521221 and EAR-1337887, and NSF EAR Instrumentation and Facilities Program grant EAR-0824974. Funds from the New York State Museum assisted in sample analysis. Much of EL's field and laboratory work was carried out under National Science Foundation grant support while at the New York State Museum. GG's field work was supported by research grant GE549/13-1 of the Deutsche Forschungsgemeinschaft, and the preparation of the manuscript was made possible by research grant GE549/22-1. Two anonymous reviewers and Fred Sundberg are thanked for helpful critiques.

**Supplementary material.** To view supplementary material for this article, please visit <https://doi.org/10.1017/S0016756820000369>

## References

- Allen CM and Campbell IH (2012) Identification and elimination of a matrix-induced systematic error in LA-ICP-MS  $^{206}\text{Pb}/^{238}\text{U}$  dating of zircon. *Chemical Geology* **332**–3, 157–65.
- Álvarez JJ, Alhberg P, Babcock LE, Bordonaro OL, Choi D, Cooper RA, Ergaliev GK, Gapp IW, Pour MG, Hughes NC, Jago JB, Korovnikov I, Laurie JR, Lieberman B, Patterson JR, Pegel TV, Popov LE, Rushton AWA, Sukhov SS, Tortello MF, Zhou Z and Žyńska A (2013) Global Cambrian trilobite palaeobiogeography assessed using parsimony analysis of endemicity. In *Early Palaeozoic Biogeography and Palaeogeography* (eds DAT Harper and T Servais), pp. 273–96. Geological Society of London, Memoir no. 38, <http://dx.doi.org/10.1144/M38.19>.
- Álvarez JJ, Bellido F, Gasquet D, Pereira MF, Quesada C and Sánchez-García T (2014) Diachronism in the late Neoproterozoic–Cambrian arc transition of North Gondwana: a comparison of Morocco and the Iberian Ossa-Moreno Zone. *Journal of African Earth Sciences* **98**, 113–32.
- Bosscher H and Schlager W (1993) Accumulation rates of carbonate platforms. *Journal of Geology* **101**, 345–55.
- Boudda A and Choubert G (1972) Sur la limite inférieure du Cambrien au Maroc. *Comptes Rendus de l'Académie des Sciences (D)* **275**, 5–8.
- Bowring SA and Schmitz MD (2003) High-precision U–Pb zircon geochronology and the stratigraphic record. In *Zircon: Experiments, Isotopes, and Trace Element Investigations* (eds JM Hanchae and PWO Huskins), pp. 305–26. Mineralogical Society of America, Virginia, Reviews in Mineralogy and Geochemistry no. 53.
- Brasier MD and Cowie JW (1989) Other areas: north-west Canada; California, Nevada, and Mexico; Morocco, Spain, and France. In *The Precambrian–Cambrian Boundary* (eds JW Cowie and MD Brasier), pp. 105–14. Oxford University Press, Monographs on Geology and Geophysics no. 12.
- Brasier MD, Magaritz M, Corfield R, Luo HL, Wu XC, Lin OY, Jiang ZhW, Hamdi B, He TG and Fraser AG (1991) The carbon- and oxygen-isotope record of the Precambrian–Cambrian boundary interval in China and Iran and their correlation. *Geological Magazine* **127**, 319–32.
- Choubert G (1952) Le Précambrien III et le Géorgien de l'Anti-Atlas. In *Contribution à l'étude du Cambrien inférieur et du Précambrien III de l'AntiAtlas marocain* (ed P Hupé), pp. 17–39. Notes et Mémoires de la Service géologique du Maroc, 103, Bagnolet, Seine.
- Compston W, Williams JL, Kirschvink JL, Zhang ZhW and Ma G (1992) Zircon U–Pb ages for the Early Cambrian time scale. *Journal of the Geological Society of London* **127**, 319–32.
- Condon DJ, McLean NM, Bowring SA and Parrish RR (2015) Metrology and traceability of U–Pb isotope dilution geochronology (EARTHTIME Tracer Calibration Part I). *Geochimica et Cosmochimica Acta* **164**, 464–80.
- Debrenne F and Debrenne M (1978) Archaeocyathid fauna of the lowest fossiliferous levels of Tiout (Lower Cambrian – southern Morocco). *Geological Magazine* **115**, 1101–19.
- Debrenne F and Debrenne M (1995) Archaeocyaths of the lower Cambrian of Morocco. *Beringeria Special Issue* **2**, 121–45.
- Debrenne F, Debrenne M and Faure-Muret A (1992) Faune d'archaéocyathes de l'Anti-Atlas (bordures nord et sud) et du Haut Atlas occidental, Cambrien inférieur, Maroc. *Géologie Méditerranéenne* **17**, 177–211.
- Eggleston JR and Dean WE (1976) Freshwater stromatolitic bioherms in Green Lake, New York. *Developments in Sedimentology* **20**, 479–88.
- Fortey RA, Briggs DEG and Wills MA (1996) The Cambrian evolutionary 'explosion': decoupling cladogenesis from morphological disparity. *Biological Journal of the Linnean Society* **57**, 13–33.
- Geyer G (1989) Late Precambrian to early Middle Cambrian lithostratigraphy of southern Morocco. *Beringeria* **1**, 115–43.
- Geyer G (1990) Revised Lower to lower Middle Cambrian biostratigraphy of Morocco. *Newsletters on Stratigraphy* **22**, 87–109.
- Geyer G (1996) The Moroccan fallotaspoid trilobites revisited. *Beringeria* **18**, 89–199.
- Geyer G (2019) The earliest known West Gondwanan trilobites from the Anti-Atlas of Morocco, with a revision of the Family Bigotiniidae Hupé, 1953. *Fossils and Strata* **64**, 55–153.
- Geyer G and Landing E (1995) The Cambrian of the Moroccan Atlas regions. *Beringeria Special Issue* **2**, 7–46.
- Geyer G and Landing E (2004) A unified Lower–Middle Cambrian chronostratigraphy for West Gondwana. *Acta Geologica Polonica* **54**, 179–218.
- Geyer G and Landing E (2006a) Latest Ediacaran and Cambrian of the Moroccan Atlas regions. In *Morocco 2006. Ediacaran–Cambrian Depositional Environments and Stratigraphy of the Western Atlas Regions. Explanatory Description and Field Excursion Guide* (eds G Geyer and E Landing), pp. 7–46. *Beringeria* Special Issue 6.
- Geyer G and Landing E (2006b) Ediacaran–Cambrian depositional environments and stratigraphy of the western Atlas regions. In *Morocco 2006. Ediacaran–Cambrian Depositional Environments and Stratigraphy of the Western Atlas Regions. Explanatory Description and Field Excursion Guide* (eds G Geyer and E Landing), pp. 47–120. *Beringeria* Special Issue 6.
- Geyer G and Landing E (2017) The Precambrian–Phanerozoic and Ediacaran–Cambrian boundary: a historic approach to a long unresolved dilemma. In *Earth System Evolution and Early Life: A Celebration of the Work of Martin Brasier* (eds AD Brasier, D McIlroy and N McLoughlin), pp. 311–49. Geological Society of London, Special Publication no. 448, doi:10.1144/SP448.10.
- Geyer G and Landing E (2018) An exploring expedition (sic) to the world's oldest trilobites. In *Proceedings of the International Conference on Ediacaran and Cambrian Sciences. Joint Meeting of International Subcommission on Cambrian Stratigraphy (ISCS) and International Subcommission on Ediacaran Stratigraphy (ISES), 12–16 August, 2018, Xi'an*, pp. 66–68.
- Harkless R and Hicks H (1871) On the ancient rocks the St. David's Promontory, South Wales, and their fossil contents. *Quarterly Journal of the Geological Society, London* **27**, 384–404.
- Harvey THP, Williams M, Condon DJ, Wilby PR, Siveter DJ, Rushton AWA, Leng MJ and Gabbott SE (2011) A refined chronology for the Cambrian succession of southern Britain. *Journal of the Geological Society, London* **168**, 705–16.
- Haslett J and Parnell A (2008) A simple monotone process with application to radiocarbon-dated depth chronologies. *Journal of the Royal Statistical Society: Series C (Applied Statistics)* **57**, 399–418.
- Hollingsworth JS (2007) Fallotaspoid trilobite assemblage from the Esmeralda Basin (western Nevada, USA). *Memoirs of the Australasian Association of Palaeontologists* **32**, 123–40.
- Hupé P (1950) Étude statistique de l'évolution du cephalon chez les trilobites Proparia et Opistoparia. *Bulletin de la Société Géologique de France* **5**, 9–24.
- Hupé P (1952) Sur les zones de trilobites du Cambrien inférieur marocain. *Comptes Rendus de l'Académie des Sciences, Paris* **235**, 481.
- Hupé P (1953a) Contribution à l'étude du Cambrien inférieur et du Précambrien III de l'Anti-Atlas marocain. *Notes et Mémoires de la Service géologique du Maroc* **103**, 402 pp.
- Hupé P (1953b) Classification des trilobites. *Annales de Paléontologie* **39**, 61–168.
- Hupé P and Abadie J (1950) Sur l'existence de Trilobites du Cambrien inférieur asiatique dans l'Anti-Atlas marocain. *Comptes Rendus de l'Académie des Sciences* **230**, 2112–13.
- Jaffey AH, Flynn KF, Glendenin LE, Bentley WC and Essling AM (1971) Precision measurements of half-lives and specific activities of  $^{235}\text{U}$  and  $^{238}\text{U}$ . *Physical Reviews C* **4**, 889–906.
- Keppie JD and Keppie DF (2014) Ediacaran–Middle Paleozoic oceanic voyage of Avalonia from Baltica via Gondwana to Laurentia: Paleomagnetic, faunal and geological constraints. *Geoscience Canada* **41**, 5–18, doi: 10.12789/geocanj.2014.41.039.
- Khomentovsky VV and Repina LN (1965) *Nizhniy kembriy stratotipicheskogo razreza Sibiri* (Lower Cambrian of the stratotype section of Siberia). Nauka, Moscow, 200 pp.
- Kirschvink JL, Magaritz M, Ripperdan RL, Zhuravlev AY and Rozanov AY (1991) The Precambrian/Cambrian boundary: magnetostratigraphy and carbon isotopes resolve correlation problems between Siberia, Morocco, and South China. *GSA Today* **1**, 69–71, 87, 88.
- Landing E (1994) Precambrian–Cambrian global stratotype ratified and a new perspective of Cambrian time. *Geology* **22**, 179–82.
- Landing E (1996) Avalon—Insular continent by the latest Precambrian. In *Avalonian and Related Peri-Gondwanan Terranes of the Circum-North Atlantic* (eds RD Nance and M Thompson), pp. 27–64. Geological Society of America, Special Paper no. 304.

- Landing E** (2005) Early Paleozoic Avalon–Gondwana unity: an obituary—response to ‘Palaeontological evidence bearing on global Ordovician–Silurian continental reconstructions’ by RA Fortey and LRM Cocks. *Earth-Science Reviews* **69**, 169–75.
- Landing E, Antcliffe J, Geyer G, Kouchinsky A, Andreas AA and Bowser SS** (2018) Early evolution of colonial animals (Ediacaran Evolutionary Revolution–Cambrian Evolutionary Radiation–Great Ordovician Diversification Interval). *Earth-Science Reviews* **178**, 105–35, doi:10.1016/j.esrrev.2018.01.013.
- Landing E, Davidek K, Westrop SR, Geyer G and Heldmaier W** (1998) Duration of the Early Cambrian: U–Pb ages of volcanic ashes from Avalon and Gondwana. *Canadian Journal of Earth Sciences* **35**, 329–38.
- Landing E, Geyer G, Brasier MD and Bowring SA** (2013) Cambrian Evolutionary Radiation: context, correlations, and chronostratigraphy—overcoming deficiencies of the first appearance datum (FAD) concept. *Earth-Science Reviews* **123**, 133–77, doi:10.1016/j.earsci.2013.008.
- Landing E, Geyer G and Heldmaier W** (2006) Distinguishing eustatic and epeirogenic controls on Lower–Middle Cambrian boundary successions in West Gondwana (Morocco and Iberia). *Sedimentology* **54**, 899–918.
- Landing E and Kouchinsky A** (2016) Correlation of the Cambrian Evolutionary Radiation: geochronology, evolutionary stasis of earliest Cambrian (Terreneuvian) small shelly fossil (SSF) taxa, and chronostratigraphic significance. *Geological Magazine* **153**, 750–57, doi:10.1017/S007675815001098.
- Landing E, Myrow PM, Narbonne GM, Geyer G, Bautois LA, Mángano MG, Kaufman AJ, Westrop SR, Kröger B, Liang B and Gougain R** (2017) Ediacaran–Cambrian of Avalonian Eastern Newfoundland (Avalon, Burin, and Bonavista Peninsulas). *International Symposium on the Ediacaran–Cambrian Transition*, Field Trip 4. The International Subcommission on Ediacaran Stratigraphy (ICES) and The International Subcommission on Cambrian Stratigraphy, St. John’s, Newfoundland, June 15–29, 2017. Newfoundland and Labrador Geological Survey, Open File, NFLD/3323, 165 p.
- Landing E and Westrop SR** (2004) Environmental patterns in the origin and evolution loci of Early Cambrian skeletalized Metazoa: evidence from the Avalon microcontinent. In *Neoproterozoic–Cambrian Biological Revolutions* (eds JH Lipps and B Waggoner), pp. 93–105. Paleontological Society, Special Paper no. 10.
- Landing E, Westrop SR and Bowring SA** (2013) Reconstructing the Avalonia palaeocontinent in the Cambrian: a 519 Ma caliche in South Wales and transcontinental middle Terreneuvian Epoch sandstones. *Geological Magazine* **150**, 1022–46, doi:10.1017/S00167681300228.
- Latham A and Riding R** (1990) Fossil evidence for the location of the Precambrian/Cambrian boundary in Morocco. *Nature* **344**, 752–4.
- Lieberman BS** (2001) Phylogenetic analysis of the Olenellina Walcott, 1890 (Trilobita, Cambrian). *Journal of Paleontology* **75**, 96–115.
- Liñán E, Gámez Vintaned JA and Gozalo R** (2008a) The middle lower Cambrian (Ovetian) *Lunagraulos* n. gen. from Spain and the oldest trilobite records. *Geological Magazine* **152**, 1123–36.
- Liñán E, Gozalo R, Dies Álvarez ME, Gámez Vintaned JA and Zamora S** (2008b) Nuevos trilobites del Ovetiense inferior (Cámbrico Inferior bajo) de Sierra Morena (España). *Ameghiniana* **45**, 123–38.
- Liñán E, Perejón A and Szalay K** (1993) The Lower–Middle Cambrian stages and stratotypes from the Iberian Peninsula: a revision. *Geological Magazine* **130**, 817–33.
- Liñán E and Szalay K** (1978) A trilobite from the Lower Cambrian of Córdoba (Spain) and its stratigraphical significance. *Senckenbergiana lethaea* **59**, 387–99.
- Linnemann U, Ovtcharova M, Schaltegger U, Gärtner A, Hautmann M, Geyer G, Vickers-Rich P, Rich T, Plessen B, Hofmann M, Ziegler J, Krause R, Kriesfeld L and Smith J** (2019) New high resolution age data from the Ediacaran–Cambrian boundary indicate rapid, ecologically driven onset of the Cambrian explosion. *Terra Nova* **31**, 49–58, doi: 10.1111/ter.12368.
- MacDonald FA, Schmitz MD, Strauss JV, Halverson GP, Gibson TM, Eyster A, Cox G, Mamrol P and Crowley JL** (2018) Cryogenian of Yukon. *Precambrian Research* **319**, 114–43.
- Magaritz M, Kirschvink J, Latham A, Zhuravlev AY and Rozanov AY** (1991) Precambrian/Cambrian boundary problem: carbon isotope correlations for Vendian and Tommotian time between Siberia and Morocco. *Geology* **19**, 847–50.
- Maloof AC, Porter SH, More JL, Dudás FÖ, Bowring SA, Higgins JA, Fike DA and Eddy MP** (2010) The earliest Cambrian record of animals and ocean geochemical change. *Geological Society of America Bulletin* **122**, 1731–74.
- Maloof AC, Schrag DP, Crowley JL and Bowring SA** (2005) An expanded record of Early Cambrian carbon recycling from the Anti-Atlas margin. *Canadian Journal of Earth Sciences* **42**, 2195–216.
- Marshall CR** (1990) Confidence intervals on stratigraphic ranges. *Paleobiology* **16**, 1–10.
- Mattinson JM** (2005) Zircon U–Pb chemical abrasion (“CA–TIMS”) method: Combined annealing and multi-step partial dissolution analysis for improved precision and accuracy of zircon ages. *Chemical Geology* **220**, 47–66.
- McLean NM, Condon DJ, Schoene B and Bowring SA** (2015) Evaluating uncertainties in the calibration of isotopic reference materials and multi-element isotopic tracers (EARTHTIME Tracer Calibration Part II). *Geochimica et Cosmochimica Acta* **164**, 481–501.
- Meert JG and Lieberman BS** (2004) A palaeomagnetic and palaeobiogeographic perspective on latest Neoproterozoic and early Cambrian tectonic events. *Journal of the Geological Society, London* **161**, 1–11.
- Meert JG and Lieberman BS** (2008) The Neoproterozoic assembly of Gondwana and its relationship to the Ediacaran–Cambrian Radiation. *Gondwana Research* **1**, 5–21.
- Mifdal A and Peucat J-J** (1985) Datations U–Pb et Rb–Sr du volcanisme acide de l’Anti-Atlas Marocain et du socle sous-jacent dans la région de Ouarzazate. Apport au problème de la limite Précambrien - Cambrien. *Bulletin des Sciences Géologiques* **38**, 185–200.
- Monninger W** (1979) The section of Tiout (Precambrian/Cambrian boundary beds, Anti-Atlas, Morocco): an environmental model. *Arbeiten aus dem Paläontologischen Institut Würzburg* **1**, 289 pp.
- Murphy JB, Nance RD, Keppie JD and Dostal J** (2018) Role of Avalonia in the development of tectonic paradigms. In *Fifty Years of the Wilson Cycle Concept in Plate Tectonics* (eds RW Wilson, GA Houseman, KJ McCaffrey, AG Dore and SJH Buiter), p. 26. Geological Society of London, Special Publication no. 470, <https://doi.org/10.1144/SP470.12>.
- Nasdala L, Christian L, Lengauer CL, Hanchar JM, Kronz A, Wirth R, Philippe Blanc P, Kennedy AK and Seydoux-Guillaume A-M** (2002) Annealing radiation damage and the recovery of cathodoluminescence. *Chemical Geology* **191**, 121–40.
- Nelson CA** (1978) Late Precambrian–Early Cambrian stratigraphic and faunal succession of eastern California and the Precambrian–Cambrian boundary. *Geological Magazine* **115**, 121–6.
- Nelson CA and Hupé P** (1964) Sur l’existence de Fallotaspis et Daguinaspis, trilobites marocains, dans le Cambrien inférieur de Californie, et ses conséquences. *Comptes Rendus de l’Académie des Sciences, Paris* **258**, 621–3.
- Neltner L** (1938) Études géologiques dans le Sud marocain (Haut Atlas et Anti-Atlas). *Notes et Mémoires du Service au Mines et Carte géologique du Maroc* **42**, 298.
- Neltner L and Pockey N** (1950) Quelques faunes géorgiennes du Maroc. *Notes et Mémoires du Service Géologique du Maroc* **2**, 53–83.
- Palmer AR and Repina LN** (1993) Through a glass darkly: taxonomy, phylogeny, and biostratigraphy of the Olenellina. *The University of Kansas Paleontological Contributions, New Series* **3**, 1–35.
- Palmer AR and Rowell AJ** (1995) Early Cambrian trilobites from the Shackleton Limestone of the Central Transantarctic Mountains. *The Paleontological Society Memoir* **45**, 1–28.
- Peng S and Babcock LE** (2005) Towards a new global subdivision of the Cambrian System. *Journal of Stratigraphy* **29**, 171–8.
- Peng S and Babcock LE** (2011) Continuing progress on chronostratigraphic subdivision of the Cambrian System. *Bulletin of Geosciences* **86**, 391–6.
- Peng S, Babcock LE and Cooper RA** (2012) The Cambrian Period. In *The Geologic Time Scale, Volume 2* (eds FM Gradstein, JG Ogg, MD Schmitz and GM Ogg), pp. 437–88. Amsterdam: Elsevier.
- Perejón A** (1986) Biostratigrafía de los Arqueociatos en España. *Cuadernos de Geología Ibérica* **9**, 212–66.
- Perejón A** (1994) Palaeogeographic and biostratigraphic distribution of Archaeocyatha in Spain. *Courier Forschungs-Institut Senckenberg* **172**, 341–54.

- Rozanov AY and Debrenne F** (1974) Age of archaeocyathid assemblages. *American Journal of Science* **274**, 833–48.
- Rushton AWA, Brück PM, Molyneux SG, Williams M and Woodcock NH** (2011) A revised correlation of the Cambrian rocks in the British Isles. Geological Society of London, Special Report **25**, 21–7.
- Schmitt M** (1979) The section of Tiout (Precambrian/Cambrian boundary beds, Anti-Atlas, Morocco): Stromatolites and their biostratigraphy. *Arbeiten aus dem Paläontologischen Institut Würzburg* **2**, 188.
- Schmitz MD and Davydov VI** (2012) Quantitative radiometric and biostratigraphic calibration of the global Pennsylvanian–Early Permian time scale. *Geological Society of America Bulletin* **124**, 549–77.
- Schmitz MD and Schoene B** (2007) Derivation of isotope ratios, errors, and error correlations for U–Pb geochronology using 205Pb–235U–(233U)-spiked isotope dilution thermal ionization mass spectrometric data. *Geochemistry, Geophysics, Geosystems* **8**, Q08006, doi: [10.1029/2006GC001492](https://doi.org/10.1029/2006GC001492).
- Sdzuy K** (1961) Das Kambrium Spaniens. Teil II: Trilobiten. *Akademie der Wissenschaften und der Literatur, Abhandlungen der mathematisch-naturwissenschaftlichen Klasse* **1961**, 499–690 (217–408).
- Sdzuy K** (1978) The Precambrian–Cambrian boundary beds in Morocco (Preliminary report). *Geological Magazine* **115**, 83–94.
- Sdzuy K** (1981) Der Beginn des Phanerozoikums — Paläobiologische und stratigraphische Probleme. *Natur und Museum* **111**, 390–99.
- Sláma J, Jan Košler J, Condon DJ, Crowley JL, Gerdes A, Hanchar JM, Horstwood MSA, Morris GA, Nasdala L, Norberg N, Schaltegger U, Schoene B, Tubrett MN and Whitehouse MJ** (2008) Plešovice zircon — A new natural reference material for U–Pb and Hf isotopic microanalysis. *Chemical Geology* **249**, 1–35.
- Stacey JS and Kramers JD** (1975) Approximation of terrestrial lead isotope evolution by a 2-stage model. *Earth and Planetary Science Letters* **26**, 207–21.
- Trayler RB, Schmitz MD, Cuitiño JI, Kohn MJ, Bargo MS, Kay RF, Strömberg CAE and Vizcaino SF** (2019) An improved approach to age-modeling in deep time: Implications for the Santa Cruz Formation, Argentina. *GSA Bulletin* 1–12, doi:[10.1130/B35203.1](https://doi.org/10.1130/B35203.1).
- Tucker M** (1986) Carbon isotope excursions in Precambrian/Cambrian boundary beds. *Nature* **319**, 49.
- Varlamov AI, Rozanov AY, Khomentovsky VV, Shabanov YY, Abaimova GP, Demidenko YE, Karlova GA, Korovnikov IV, Luchinina VA, Malakhovskaya YE, Parkhaev PY, Pegel TV, Skorlotova NA, Sundukov VM, Sukhov SS, Fedorov AB and Kipriyanova LD** (2008) The Cambrian System of the Siberian Platform. Part 1: The Aldan-Lena region. In *XIII Field Conference of the Cambrian Stage Subcommittee Working Group*. Yakutia, Russia, July 20–August 1, 2008. Moscow, Novosibirsk: PIN Russian Academy of Science, 300 p.
- Walsh GJ, Aleinikoff JN, Benziane F, Yazidi A and Armstrong TR** (2002) U–Pb zircon geochronology of the Paleoproterozoic Tagragra de Tata inlier and its Neoproterozoic cover, western Anti-Atlas, Morocco. *Precambrian Research* **117**, 1–20.
- Wendt I and Carl C** (1991) The statistical distribution of the Mean Squared Weighted Deviation. *Chemical Geology* **86**, 275–85.
- Williams M, Rushton AWA, Cook AF, Zalasiewicz J, Martin AP, Condon DJ and Winrow P** (2013) Dating the Purley Shale Formation, Midland microcraton, England. *Geological Magazine* **150**, 937–44.
- Zhuravlev AYu** (1995) Preliminary suggestions on the global Early Cambrian zonation. *Beringeria Special Issue* **2**, 147–60.